

UNIVERSITY OF CENTRAL OKLAHOMA

Edmond, Oklahoma

College of Graduate Studies and Research

**DESIGN CRITERIA OF A TRANSCUTANEOUS POWER DELIVERY
SYSTEM FOR IMPLANTABLE DEVICES**

A THESIS

SUBMITTED TO THE GRADUATE COLLEGE

In the fulfillment of the requirements for the degree of

MASTER OF SCIENCE IN ENGINEERING PHYSICS

By

Shams Shahadat

Edmond, Oklahoma

2012

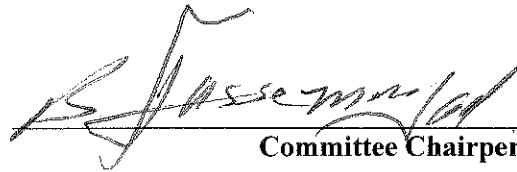
**DESIGN CRITERIA OF A TRANSCUTANEOUS POWER DELIVERY
SYSTEM FOR IMPLANTABLE DEVICES**

A THESIS

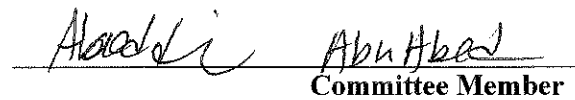
APPROVED FOR THE DEPARTMENT OF ENGINEERING AND PHYSICS

11/20/2011

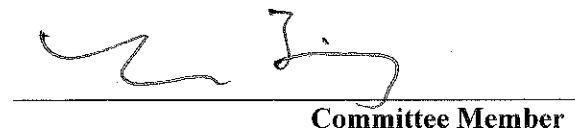
By



Committee Chairperson



Committee Member



Committee Member

ACKNOWLEDGMENTS

I would like to extend my sincere gratitude to my advisor, Dr. Baha Jassemnejad, for his support and excellent guidance in this research. I consider myself very fortunate to have had the opportunity to have him as my academic mentor as his teachings will forever motivate me to pursue higher studies. I would like to thank Dr. Alaeddin Abu-Abed and Dr. Yuhao Jiang for serving as member of my supervising committee. I would also like to appreciate Dr. Ryan Stanfield and Dr. Trevor Snyder for providing guidance in this research. I would also like to acknowledge the Student Research, Creative, & Scholarly Activities (RCSA) Grant Program at University of Central Oklahoma (UCO), Edmond, Oklahoma for supporting this research project. I would also like to thank my parents who are always there for me with endless love and encouragement. In addition, I would like to thank my three sisters for their devoted love and support throughout my academic career. Finally, I would also like to thank the fellow graduate and undergraduate students and the rest of faculty and staff of Department of Engineering and Physics for making my experience at UCO a pleasant one.

TABLE OF CONTENT

Acknowledgment	iii
Table of Contents	iv
List of Figures	vi
List of Tables	ix
Abstract	1
Introduction	3
Chapter 1: Wireless Power Transmission	6
1.1 Introduction	6
1.2 Power Transmission using Electromagnetic Induction	6
1.3 Ultrasonic Power Transmission	7
1.4 Power Transmission using Resonance Induction	8
1.5 Long Distance Power Transmission	9
1.6 Summary	9
Chapter 2: Transcutaneous Power System	11
2.1 Introduction	11
2.2 Power Flow Control	13

2.3 Previous Systems	15
2.3.1 Inductive Charging with TET System	16
2.3.2 Resonant Coupling with FREE-D System	16
2.3.3 Clinical Results	18
2.4 Summary	20
Chapter 3: Power Transfer Topology	21
3.1 Introduction	21
3.2 Electromagnetic Compatibility	21
3.3 Circuit Design	23
3.3.1 DC Converter	23
3.3.2 Tuning Topologies	25
3.4 Summary	31
Chapter 4: Optimized Geometry of Transcutaneous Coils	32
4.1 Introduction	32
4.2 Electromagnetic Induction	32
4.3 Coupling and Mutual Inductance	34
4.4 Coil Alignment Scenarios	36
4.5 Summary	45

Conclusion	46
References	48
Appendix A	59
Appendix B	60

LIST OF FIGURES

Fig. 1: The AbioCor Total Artificial Heart (TAH) with its TET System	3
Fig. 2: Tethered Power Line Supported Percutaneous System	12
Fig. 3: Skin-cable Exit Site on the Abdominal Wall	12
Fig. 4: Power Flow Diagram of a Transcutaneous Power System	13
Fig. 5: Power Controller Topology with Feedback Control using Phase Locked Loop	15
Fig. 6: FREE-D System	17
Fig. 7: Diagrammatic Comparison of Converters with Approximate Limits of Application	24
Fig. 8: Voltage Driven Generalized Model of Inductive Link	27
Fig. 9: No Resonance Topology	27
Fig. 10: Series Tuned Primary Topology	27
Fig. 11: Series Tuned Secondary Topology	28
Fig. 12: Series Tuned Primary and Secondary Topology	28
Fig. 13: Parallel Tuned Secondary	28
Fig. 14: Series Tuned Primary and Parallel Tuned Secondary Topology	28
Fig. 15: Electromagnetic Induction	33
Fig. 16: Arbitrary positioning of the Secondary Coil	36

Fig. 17: Secondary coil is parallel and center aligned separated by vertical distance	38
Fig. 18: Secondary coil center aligned with an inclined angle	38
Fig. 19: Secondary coil is parallel and has a lateral alignment	38
Fig. 20: Secondary coil has a lateral alignment with inclined angle	39
Fig. 21: Secondary coil is rotational in a lateral alignment with inclined angle	39
Fig. 22: Vector Potential of Primary Loop with reference to Secondary Loop	39
Fig. 23: Behavior of f with respect to k^2 in Calculation of Mutual Inductance	41
Fig. 24: Behavior of f with respect to k^2 - Logarithmic Approximation	42
Fig. 25: Behavior of f with respect to k^2 - Distributed Approximation (Grover)	42
Fig. 26: Behavior of f with respect to k^2 - Distributed Approximation (RF Handbook)	43

LIST OF TABLES

Table 1: Comparative performance evaluation between TETS and FREE-D Systems	17
Table 2: Approximation of Proportionality Factor f within k' Range by Several Physicists	41
Table 3: Grover's Approximation Data Set for k'	59
Table 4: RF Handbook Approximation Data Set for k'	60

ABSTRACT

Implantable cardiac assist devices such as artificial hearts and blood pumps are a rapidly growing therapy used for treating moderate to severe congestive heart failure. While current treatments offer improved heart failure survival and increased patient functionality with enhanced quality of life, powering these devices are still constraining. In practice, percutaneous cables passing through skin are used for power and control data transmission requiring patients to maintain a sterile dressing on the skin cable-exit site. This contact site limits patient movement as it is vulnerable to wound infection due to trauma and poor healing. As a result, a sterile dressing has to be maintained and nursed regularly for treating the wound. Complications from the exit site infections are a leading cause of death in long-term support with these devices. Wireless power and control transmission systems have been studied and developed over years in order to avoid percutaneous cables while supplying power efficiently to the implanted device. These power systems, commonly named Transcutaneous Energy Transfer (TET) systems, enable power transmission across the skin without direct electrical connectivity to the power source. TET systems use time-varying electromagnetic induction produced by a primary coil that is usually placed near skin outside the body. The induced voltage in an implanted secondary coil is then rectified and regulated to transfer energy to an implanted rechargeable battery in order to power the biomedical load device. Efficient and optimum energy transfer using such transcutaneous methods is more complex for mobile patients due to coupling discrepancies caused by variations in the alignment of the coil. The research studies equivalent maximum power transfer topologies for evaluating voltage gain and coupling link efficiency of TET system. Also, this research adds to previous efforts by generalizing different scenarios of misalignments of different coil size that affects the coupling link. As a whole, this study of geometric coil

misalignments reconsiders potential anatomic location for coil placement to optimize TET systems performance in anticipated environment for efficient and safe operation.

INTRODUCTION

Advances of technological breakthrough in wireless power delivery to implantable biomedical devices have motivated numerous academic and industrial researches over the years. Several noteworthy developments of innovative low-power circuits and power systems have been implemented and tested for powering implantable devices to ensure improved progress in destination therapy [1]. The traditional approach to supplying power using percutaneous wires tethered from power source is susceptible to infection and irritation on contact skin [1]-[8]. Medical research documentation shows that patients developing skin related infections have multiple readmissions and spend more time in the hospital [2],[5]. Therefore, transcutaneous methods [3],[4],[7]-[21] are designed to avoid piercing of skin using two loosely coils separated by skin distance for power delivery. These transcutaneous coils are generally designed in size and shape in order to have functionality similar to that of an air-coil transformer.

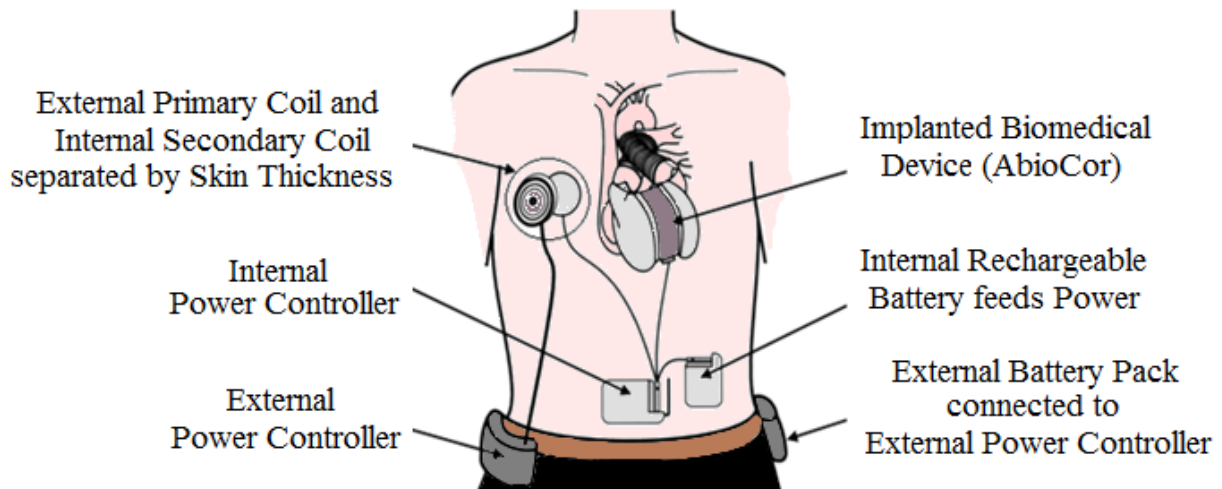


Fig. 1: The AbioCor Total Artificial Heart (TAH) with its TET System

(Reproduced from Journal of Cardiac Surgery) [7],[21]

In a TET system for an artificial heart mechanism, as shown in Fig. 1, the primary coil is resided outside of the human body, and is excited by an alternating current. The secondary coil is placed just beneath the skin inside the body to receive the transmitted power. Fluctuating magnetic flux generated from the primary coil interacts with the secondary coil through dermal skin depth. As a result, an unstable sinusoidal voltage is induced at the receiving coil, which is rectified and regulated for power delivery to a rechargeable battery. Even though the battery makes the implanted system quite bulky, it is purposed for continuous and safer operation of the biomedical device [7]. The overall system design is meant for the battery to recharge using separate wireless chargers employing the same technique that is used for rechargeable toothbrushes and cell phone charging pads. The load device is usually placed very close to the transmitting coil for such charging systems. This is mainly because the efficiency of power transfer is affected by the distance between the transmitter and receiver coils. Another point of interest constraining the design is the regulation of continuous power causing unwanted temperature increase of the coils that may cause tissue damage [16],[20].

The tissue surrounding the coils has a finite capacity to dissipate any heat generated; however, increase in the skin temperature beyond 1°C or 2°C for excessive time is considered unsafe as it can lead to chronic tissue damage [4],[9],[22]. Placement of the coils on the body is another concern as it can hamper patient movement. Furthermore, accumulation of fat over the long-term below skin can also be speculated for affecting the efficiency of power delivery. In light of overcoming such constrictions during destination therapy as well as designing efficient systems, this research presents an overview of different systems and general methods that have been adopted and studied by researchers for powering implantable devices wirelessly. This research presents an overview study of transcutaneous power systems for implantable devices

while theoretically emphasizing the impact of link efficiency of a system with respect to the size of the coils and their oriental geometry of alignment. Comprehension of these alignments can be utilized to define coupling link efficiency as well as the mutual inductance between the coils.

The scope and structure of the thesis is motivated towards wireless energy transfer. Chapter 1 highlights distinctions in application and configuration of different wireless energy transfer methods that have been studied and developed over years. Clinical results and recent progress of TET systems are reviewed in Chapter 2. Next, performance of different equivalent topologies for maximum power transfer is presented in Chapter 3. In the end, Chapter 4 utilizes coil sizes and geometric orientation of alignment to determine coupling factor of the transcutaneous coils by using commendable computational methods to calculate mutual inductance.

CHAPTER 1

WIRELESS POWER TRANSMISSION

1.1 Introduction

It has taken over 100 years to explore wireless transmission with the progress development of electronics and information technology. Heinrich Hertz and Nicola Tesla were initially able to theoretically validate the possibility of wireless power transmission at the end of 19th century. In late 1899, Tesla had devised a type of resonant transformer, now referred as the Tesla coil, that was able achieve a major breakthrough by transmitting electric power wirelessly over distance ranging in miles to light up a bank of light bulbs and run an electric motor. However, the detrimental effects of transmitting such high voltages in electric arcs are harmful to humans and electrical equipment in the vicinity. Throughout the years, a good many number of research and successful business applications has been achieved in both domestic and international frontiers. Yuwei et al. [23] have accumulated well documented progress of wireless transmission methods that are currently in practice in modern days. These methods can be categorized in the following.

1.2 Power Transmission using Electromagnetic Induction

Electromagnetic induction is a short distance mode of wireless power transmission that ensures the furthest distance of power transmission within several millimeters to centimeters. The typical representation of electromagnetic transmission mode is based upon electromagnetic induction theory. Also known as induction power transmission, electromagnetic induction adopts a non-contacting transformer consisting of detachable a primary and a secondary coil wind. The winds are separately coiled around different magnetism framework to transfer power through

nonmagnetic material. Inductive power transfer using AC power mainly depends on its frequency because the AC power directly proportional to its frequency. Therefore, it is necessary to maintain a high operating frequency to overcome transmission loss for inductive power transfer. This mode of wireless power system can transmit hundreds of kilowatt rated power, making this inductive power transmission fit for high power wireless transmission. Experimentally, the transfer efficiency can reach as high as 70% while rest of the power loss is compromised due to other system constraints. Beyond this range, efficiency decreases significantly, which makes it difficult choice for practical application. So, inductive power transmission is appropriate for short distance for low or high power requirement wireless transmission. Presently, application of inductive power transmission have been widely explored with a focus on wireless charging system of many household electronic commodities as well as medical treatment equipment.

1.3 Ultrasonic Power Transmission

Ultrasonic power transmission is categorized in middle distance transmission mode [23]. The furthest distance of a general middle distance mode can be extended to several meters. Ultrasonic functions as a sound wave with a frequency of more than 20 kHz. Research in application of power ultrasonic technology has achieved comparative development with respect to other wireless power transmission techniques. Ultrasonic power transmission has been practically applied for research in ultrasonic machining and processing technology for detection and control of ultrasonic energy. Ultrasonic power transmission exploits characteristics of piezoelectric effect and converse piezoelectric effect of piezoelectric material. Piezoelectric materials have the capabilities to convert mechanical power to electrical power and vice versa. This system firstly converts AC source from sine wave to pulse that is magnified by an amplifier.

Then the power is sent into an ultrasonic transducer to realize conversion of electrical power to ultrasonic power for transmission. The converse process of production of ultrasonic is then applied to convert the energy to electrical energy. Finally, power commutation and regulation procedures are adopted to improve quality for power delivery to load circuit. The research in ultrasonic wireless power transmission is mainly focused on small power wireless charging system as the efficiency of this method largely depends on the size and quality of piezoelectric material being used.

1.4 Power Transmission using Resonance Induction

When transmission distance is relatively long, transmission efficiency of inductive power transmission mode is very low, and receiver can only receive a very small amount of power. Researchers have invented a completely novel wireless power transmission method based on resonance induction technology by implementing maximum power transfer topology. Resonance induction is almost similar to inductive coupling except intrinsic frequencies of receiving antenna coil are in accord with electromagnetic field frequencies of sending antenna coil of a resonating transformer. Electrical power transmission efficiency is quite high for resonance induction, and power can be transferred successfully between 3-4 meters [5], [23] of distance with a power rating up to several kilowatts. Currently, resonance wireless power transmission has been used for wireless charging of mobile phones, notebooks, computers, and other household electrical equipment. The present problem existing in this application is mainly drawbacks of over-sized receiver and transmitter coils.

1.5 Long Distance Power Transmission [23]

Long distance wireless power transmission is meant to reach several decades of kilometers. This is achieved by using microwave and laser transmission. Microwave is one kind of electromagnetic wave, whose wavelength is from 1mm to 1m, with frequency ranging from about 0.3 GHz to 300 GHz [24]. The discovery of microwave conversion to DC power resolved a long time problem that paved the way for the development of microwave wireless power transmission. As the wavelength is comparatively long, microwave produces large scattering in long distance transmission resulting in poor power transmission. Microwave wireless power transmission applications are very limited to wireless charging of space-based solar power system and satellite solar power system as it needs bigger sending and receiving antenna like the size of a several storied building. On the other hand, laser power transmission is used for its application for better directional property and high power carrying capability. Laser has a better directional property than common light source. Scattering is the primary disadvantage of laser power transmission. The realization theory of laser power transmission is simple and quite similar to a common laser generator. Research focus in application for laser wireless power transmission is similar to microwave power transmission as they both require direct line of sight with the receiving target. In addition to its limited application, there are alarming drawbacks of using wireless laser power transmission as it is hazardous to human and animals even at low power levels.

1.6 Summary

In comparison with traditional power systems that use power drive lines, wireless power transmission has become research focus for scientist all around the world. The noted wireless power transmission methods have been realized in numerous commercial applications and

brought much convenience to many aspects of daily life, while other complex systems are still under study to expand the horizon of wireless power systems. In case of powering implantable biomedical devices, microwave and laser power transmission is inapplicable. Technology of using implanted piezoelectric material for receiving non-invasive ultrasonic power is debated and offers prospects for future development. Clearly, powering implantable devices using inductive and resonance coupling has achieved remarkable progress over the years. Numerous systems designs and implementation have been validated for performance testing of inductive and resonant power devices that are relatively appropriate for powering biomedical implants. Empirical studies from several clinical trials show that use of wireless systems used for powering implants has lower the cost of care-delivery as well as improved patient quality of life to a large extent [5]. This research is an effort to contribute to the study of inductive and resonant power systems for its application in transcutaneous energy transfer systems for cardiac assist devices, mainly mechanical circulatory support and blood pumps for the heart.

CHAPTER 2

TRANSCUTANEOUS POWER SYSTEM

2.1 Introduction

Implantable biomedical devices have found applications in a wide range of areas, including pacemakers, cochlear implants, physiological monitoring devices, drug infusion devices, functional electrical stimulators, left ventricular assist devices (LVAD), and artificial hearts. Implantable batteries are traditionally used with percutaneous links for power delivery. However, reliability problems of limited energy storage and life span of the battery and infection susceptibility of percutaneous power drive-line as shown in Fig. 2 and Fig. 3 inspires study of wireless power systems that can be designed to provide power continuously without the risk of infection from the percutaneous lead. Empirical studies show [1],[2],[5],[7],[8] that longest surviving patients of nearly 7 years with percutaneous systems have been found to be readmitted to hospital for treatment of infection on skin-cable exit site. As a result, patients have to spend more time in the hospital that contributes significantly to the cost of care-delivery. Research in transcutaneous power systems is primarily motivated to remedy these disadvantages of percutaneous system with the intention of improving aspects of technical design for transferring power wirelessly. This chapter addresses general technical properties of a point-of-interest TET system with respect to previous systems that have been developed and trialed over the decades.

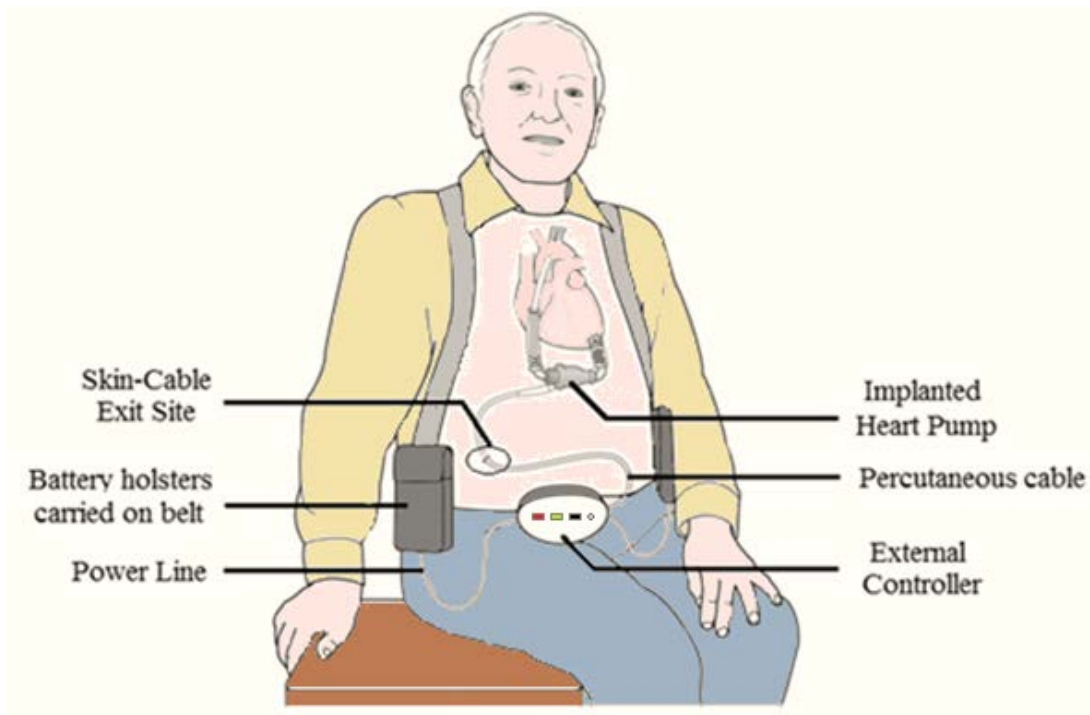


Fig. 2: Tethered Power Line Supported Percutaneous System

(Reproduced from AARP Health)

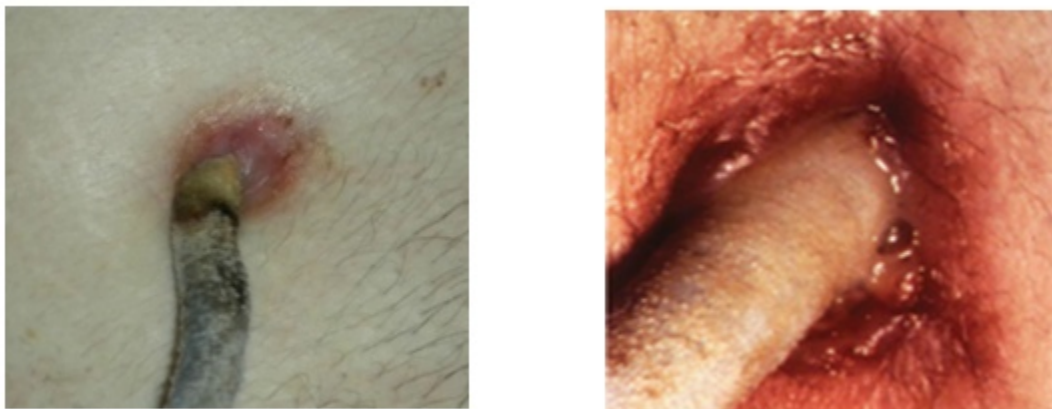


Fig. 3: Skin-cable Exit Site on the Abdominal Wall

(Image Courtesy: The Website for Cardiovascular Specialists)

2.2 Power Flow Control

Similar technology of transcutaneous power delivery systems for powering implanted artificial heart mechanism as illustrated in Fig.1, have been widely studied in diverse medical applications. Cochlear implants [25], BION devices [26] and nerve stimulators [27],[28], retinal prostheses [19],[29], knee prostheses [30], and drug infusion delivery systems [31],[32] are only to name a few of such applications. In consideration of these applications, a customary power flow diagram is shown in Fig. 4 that represents general functionalities of both external and implanted system of such transcutaneous power systems.

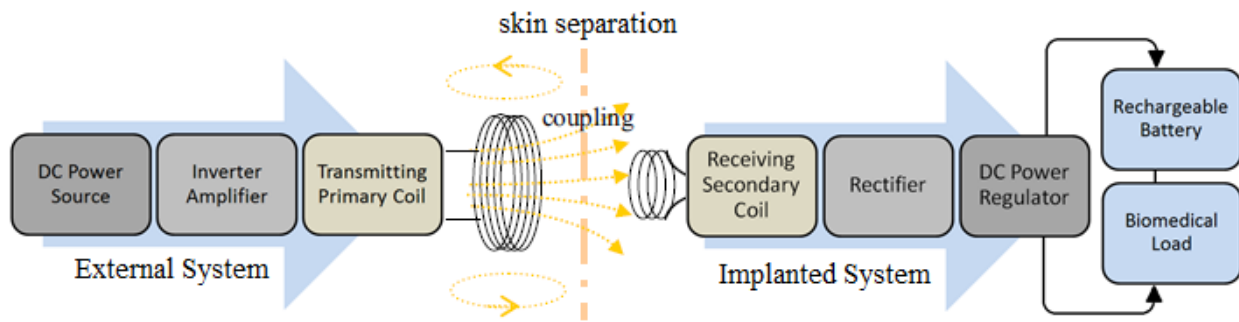


Fig. 4: Power Flow Diagram of a Transcutaneous Power System

Functional designs of the both external and implanted system are mostly inspired by the obligation to supply maximum power while addressing solutions to medical problems in therapeutic stages of treatment. Different control and feedback systems have been implemented to either or both external and implanted systems to improve overall efficiency of the power system. Generally, all power transfer topologies are designed utilizing principles of maximum power transfer which requires controlling the operating frequency on both primary and secondary circuits. Maximum power transfer occurs as:

Impedance of Primary Circuit = Impedance of Secondary Circuit

and

Operating Frequency of Primary Circuit = Operating Frequency of Secondary Circuit

Traditional TETS controller regulates power using two main methods. Firstly, a voltage control method is designed to control the input voltage amplitude to deliver demanding power. Though this is a very common method, it fails to take into account the miss-match of the operating frequency of the resonating circuit. This miss-match in frequency reduces the power transferred in a voltage control method because this requires a larger input voltage. Therefore, a frequency control method is adopted that involves varying the impedance of the primary and secondary circuit to stabilize the power delivered to the rechargeable battery. The frequency miss-match information is fed to the external controller so that the receiving voltage and resonant frequency on the secondary pick-up is either tuned or detuned by the controller. A Radio Frequency - RF link wireless system is often used for providing feedback communication between the external controller and implanted circuits. The receiving alternating power on the secondary coil is regulated and compared using several techniques such as Phase-Locked-Loop phase detection – (PLL PD), regulated voltage comparator buffer in order to distinguish and feed frequency miss-match information to the controller. Fig. 5 shows a general control system implemented for a typical TET system that uses a PLL PD. The controlled power on receiving coil is rectified by techniques such as half wave diodes, full-wave diode bridge etc. that are suitable to meet specifications of desired DC power regulation. The rectified voltage is consequently regulated to model and stabilize energy supply to a rechargeable battery.

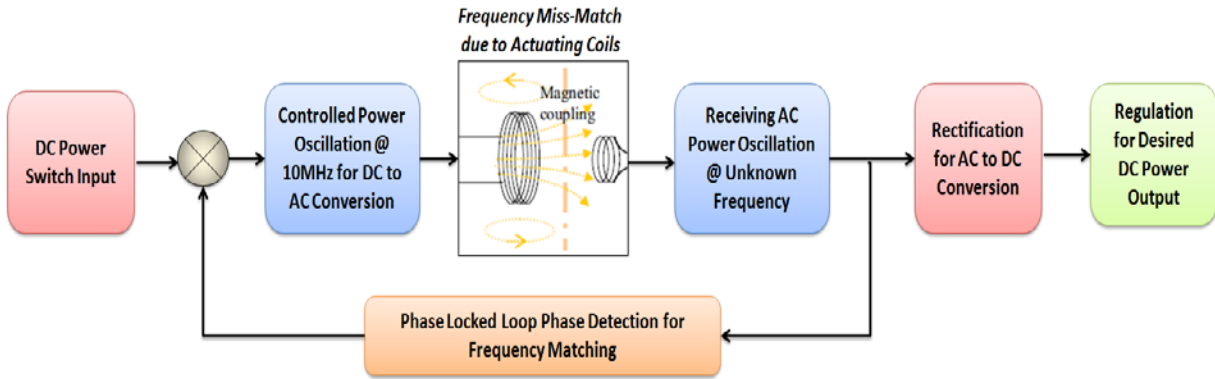


Fig. 5: Power Controller Topology with Feedback Control using Phase Locked Loop

Higher frequency control along while using a smaller secondary coil design ensures better and efficient power transfer for TETS. Continuous and efficient power supply rate to the rechargeable battery is mostly achieved by controlling current supply duty cycle. Better duty cycle control is achieved by use of fast switch drivers functioning in MHz frequency range. Such switch-mode converters and amplifiers are MOSFET switch driven controllers; therefore, they need high drive requirement for functioning. This means that the complex test circuits draw relatively excess power from the main power source. Regardless of different power controller design, the main purpose of the controller is to adjust circuit parameters for impedance matching in order to establish a power transfer-link between the external and internal coils.

2.3 Previous Systems

In recent years, the power systems are designed to transfer maximum power through skin based on the two principle methods. Both methods have been successfully implemented for trial with modified controller settings satisfying maximum power transfer requirement to maintain a specific operating frequency both in the primary and the secondary circuit.

2.3.1 Inductive Charging with TET System

Transcutaneous energy transfer systems (TETS) using inductive charging have been well explored with several decades of prototype development and laboratory testing. Ever since the first clinical treatment using Arrow LionHeart, and consequently ABioCor TAH, documented progress of clinical applications of TETS have clarified the essential need for further improvement in this field of research [7],[33],[34]. The gradual shortcoming of TETS system is the practical restriction for efficient power supply due to misalignment of the transmitting and receiving coils. The transmitter controller of TETS system is usually designed to supply more power to compensate for the vigorous oriental misalignment of the coils. This misalignment is mostly caused due to active patient contact that requires maintaining of the primary coil in a single position on the skin surface near the implant coil.

2.3.2 Resonant Coupling with FREE-D System [5]

Free-range resonant electrical energy delivery - FREE-D system uses strong resonant coupling to supply power to any load. In contrast to TETS system, FREE-D system primary and receiving coils are auto tuned to resonate at a specific frequency, which makes it a better method to supply power effectively regardless of oriental misalignment of the coils. FREE-D system promisingly envisions using several relay resonators powered by a source primary coil. This automatic tuning technique of FREE-D system combined with relay resonators is fundamentally designed to overcome the shortcoming of misalignment of coils in TETS system. Noteworthy research shows that a FREE-D system can transfer power efficiently over a range of meters compared to several centimeters proximity limitation of a TETS system. However, the energy transfer range and performance for both FREE-D and TETS systems strictly depend on the size

of the resonating coils. The following shows a performance evaluation between TETS and FREE-D systems [5], [8].

Efficiency		FREE-D System	TET System
> 50%	Separation Distance	120.0 cm	6.4 cm
	Angular Misalignment	83°	10°
< 10%	Separation Distance	160.0 cm	10.0 cm
	Angular Misalignment	88°	12°
Primary Coil Diameter		31 cm	85 mm
Energy Transfer Range		Meters (relay resonators)	10.0 cm

Table 1: Comparative Performance Evaluation Between TETS and FREE-D Systems by Bonde et.al [5]

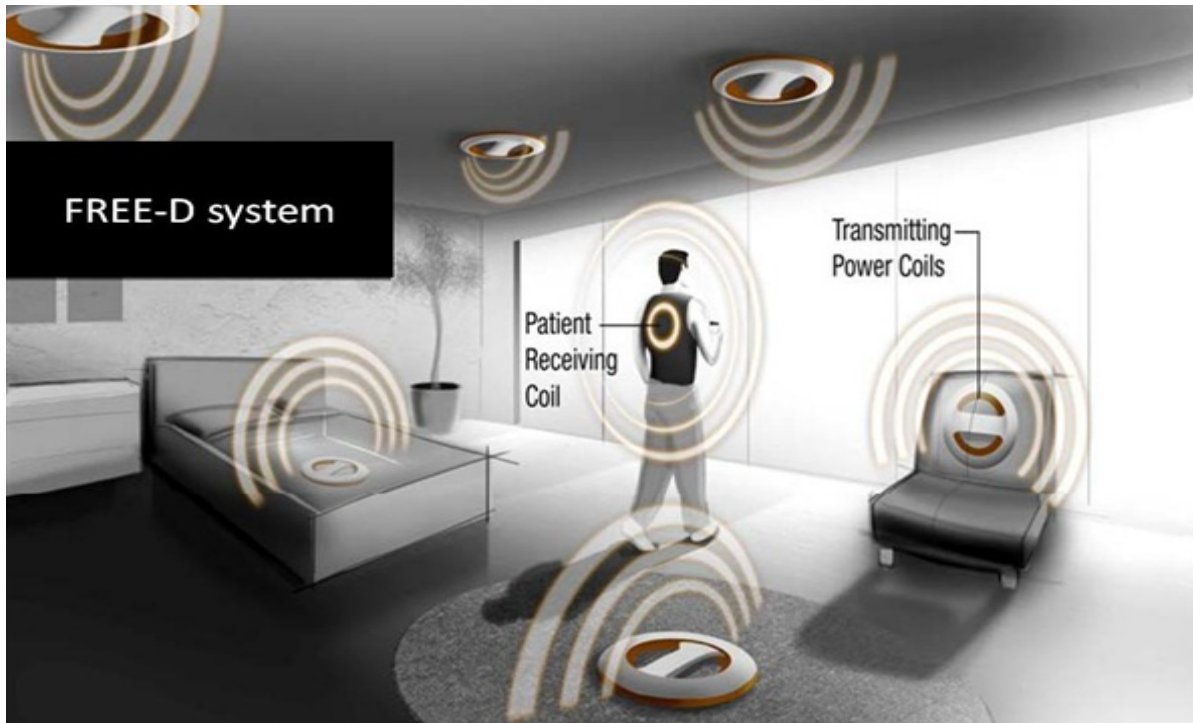


Fig.6: FREE-D System

(Image Courtesy: Bonde et al., Yale School of Medicine)

2.3.3 Clinical Results [1], [2], [3], [5], [7], [8], [23]

Many of the long-term cardiac support systems in clinical use today are the product of nearly 50 years of research and development efforts. The ultimate goal in this field of research has been to develop a totally implantable wireless power system without penetrating skin by power drive-line. The development of a reliable, internal electrical power supply using batteries has been considered and implemented for many biomedical implant devices such as pacemakers and defibrillators. However, replacing batteries for these implanted devices is also life-threatening due to consequences of critical surgery requirements. Electrically driven cardiac support devices usually require a continuous power supply of at least 8W to 12W (12V @ 0.7Amp). Conventional batteries are not capable of providing this amount of power for more than about half an hour. Therefore, several methods for transcutaneous systems were developed ever since the origination of TET system in 1960. A trial with canine experiments was demonstrated proving that an implanted artificial heart mechanism can be operational using a wireless power system. It also proved that TET system concept is viable as long as it is found to be safe and harmless to the animal. This paved the way for human trial treatments. Later, several TET systems were developed with their totally implantable LVAD and TAH implants for clinical use. Although, TET systems had been fully developed and tested many years before, a TET system was not used clinically with a LVAD until 1999 and with a TAH until 2001 [7].

The primary principle implemented in the first TET system was based on the inductive coupling between an external primary coil and an internal secondary coil. The secondary coil was placed subcutaneously in the upper interior chest wall, and the primary coil was located on the surface of the skin just right on top of the secondary coil. The secondary coil wind shaped like a dome so that when it was implanted a raised area of skin is visible on the upper chest wall.

Therefore, the primary coil wind was usually placed in close proximity to maintain adequate coupling between the two coils. A patient usually carries or wears batteries on a belt that are attached to a TET system control unit. This DC battery power is converted for AC excitation of the primary coil. In general experimentation, a TET system can provide 70W to 80W of power depending on the power of the source battery while functioning properly within a range of skin thickness of 3-15 mm and a misalignment of the coils by as much as 20 mm. The efficiency of the power transfer is adversely affected by axial and radial positioning of the primary and secondary coils. The power transfer efficiency is important because the energy loss forms into heat generation which could be potentially dangerous to the patient. Two possible sources of heat generation had been considered – heat generation by the coils and heat generation by the implanted electronics. The generated heat from the electrical equipment is dissipated to its biocompatible casing. Heat generated by the coils depends on the duration and the efficiency of the coupling between the coils. Also, low efficiency reduces the time for an external battery to support the device. Therefore, proper coupling of the TET coils is vital to keep the implanted device operating safely and continuously while maintaining an adequate charge in the implanted rechargeable battery. For a complete non-tethered system, generally needed for activities such as bathing, swimming, and other mobile activities, an implanted control unit and an internal, rechargeable battery is designed to control and supply power for durations ranging from 30 minutes to 1.5 hours [7],[8]. With these system specifications, many clinical complications of TET systems have motivated design of present transcutaneous power systems.

Clinically tested wireless power systems such as AbioCor TAH and LionHeart LVAD have been well documented over the years. The AbioCor TAH has been under trial with patients under treatment for biventricular failure. The first LVAD pump initially required a percutaneous

driveline, meaning a biocompatible cable penetrated the body to connect the pump to a power source and the system controller. A similar system is shown in Fig. 3. VAD have been reported to treat patients for upwards of 5 years [7]. As a result of the extended lifetime of the percutaneous VAD, the most common cause for patient readmission to the hospital and patient death is no longer the technical failure of the VAD, but rather the exit site infection from the percutaneous driveline. The increasing risk of infection hampers the patient's quality of life and lead to repeated hospitalizations for antibiotic treatment, surgical interventions, or even a total costly replacement of the biomedical implant. The net result of these complications from infection of the exit site is the reduced survival and increased cost which negates the intended benefit of VAD therapy. Therefore, totally implantable TET system LionHeart 2000 LVAD has been implanted for patient treatment. Although the device-related infection rate was lower, device failures and neurologic events were responsible for the worsened morbidity and mortality rates [7]. Occasional loss of power to the implanted components has been reported due to the placement of secondary coil too deep below the skin.

2.4 Summary

Although neither the AbioCor nor LionHeart clinical studies achieved good long-term survivals, the studies does show progress in reducing the incidence of device-related infections, The infection on the exit site continues to be a limiting factor for all implanted circulatory support devices. In both studies, the TET system was reliable, and any problems encountered were technical and found resolvable. In addition to solving these problems, fundamental goal of ensuring improved quality of patient life motivates design criteria of a wireless power system for an implantable biomedical device.

CHAPTER 3

POWER TRANSFER TOPOLOGY

3.1 Introduction

Wireless power systems are specifically designed to meet power requirements of implanted target devices. Developing trendy portable external systems with compact implant devising have been one of the focal aspects of research in this field in recent years. Conventional scheme of a wearable external DC battery pack is used as a main power source for the overall system. This DC power is then converted to AC power in order to excite the primary coil. The mutual coupling between the primary and secondary coils produces a vibrant sinusoidal voltage in the pickup coil which is rectified and regulated to output a stable DC power. Any theoretical determination of these circuit system designs depends on the characteristics of the pickup voltage and the use of low-power electrical circuit components. There are several constraints that require prior attention for designing a safe TET system such as the electromagnetic capability.

3.2 Electromagnetic Compatibility

The study of electromagnetic compatibility of TETS addresses two viewpoints. Firstly, it should not induce harmful effects to the patient's health and secondly, it must function properly without influence due to interference from nearby electronic equipment. The former being considered most important, empirical studies show that magnetic field generated by the external coil will impact tissue heating that require some concern about safety regulations for designing a TETS. Previous studies report that working TETS produces maximum of 6°C temperature change [20]. Furthermore, recognized studies in energy absorption of tissue are considered a

much more realistic parameter than tissue heating. Energy absorption of tissue is defined using magnitude of SAR (Specific Absorption Rate).

$$\text{SAR} = \sigma E^2 / 2\rho \quad \text{units in Watt/Kg}$$

Where, σ = electrical conductivity of the medium

E = dissipated energy

ρ = mass density

ANSI (American National Standards Institute) along with IEEE used SAR to set standards in this case [35]. For safety concerns, 1g of tissue in cubic shape, SAR should not exceed 8 Watts/Kg; whereas, for ankles, wrists, hands, feet averaging 10g of tissue should not exceed 20 Watts/Kg [35]. Exposures in excess of the standards may not be harmful but are not recommended. As a result, these restrictions help determining the operating frequency of TETS design to satisfy FCC (Federal Communication Commission) standards. In this respect, studied TETS have been designed with higher operating frequencies ranging below 30 MHz.

Furthermore, electromagnetic radiation can be divided into two different types: ionizing and non-ionizing. Ionizing radiation is radiation that has sufficient energy to remove electrons from atoms. Depending on the level of exposure, this can cause serious health problems such as increasing the possibility of cancer or harmful genetic mutations. Non-ionizing radiation includes the spectrum of ultraviolet, visible light, infrared, microwave, radio-frequency, and extremely low frequency. The main effect of non-ionizing radiation is the heating of tissues due to the absorption of electromagnetic energy. This heating of tissues has been known to have side-effects including the inductions of opacities of the lens of the eye, possible effects on development and male fertility, various physiological and thermoregulatory responses to heat, and decreased ability to perform mental tasks. Epidemiological research in studying relationship

between electromagnetic energy and biological disorders endorse wireless power delivery systems as long as they do not cause electromagnetic interference with other nearby electronic equipment and most importantly, operate safely without inducing harmful radiation effects to patient health.

3.3 Circuit Design

Our point-of-interest implantable device is generalized to require about 12V-0.7Amp power for functioning. TETS systems that directly supplies power to implantable device fails to supply power continuously due to inefficient electromagnetic coupling of coils. As a result, use of an internal rechargeable battery is idealized as a primary implanted device for TETS. This battery reduces power latch ups and can feed power to other implanted device continuously. The most commonly used circuit design used for TETS is frequency controlled series tuned primary and parallel tuned secondary transformer power topology. These topologies have different design classifications that are used for TETS. General overviews of these design classification are presented here as whole.

3.3.1 DC Converter

Various converters have been considered for wireless power systems to improve efficiency under limits of application requirements. Fig. 7 [36] shows a diagrammatic comparison of different converter principles with their approximate limits of application to meet power demand of load devices. As shown, the enclosed region within OPQRO up to 50V and 50W, low output power applications can be designed with regular step-up or fly-back converters.

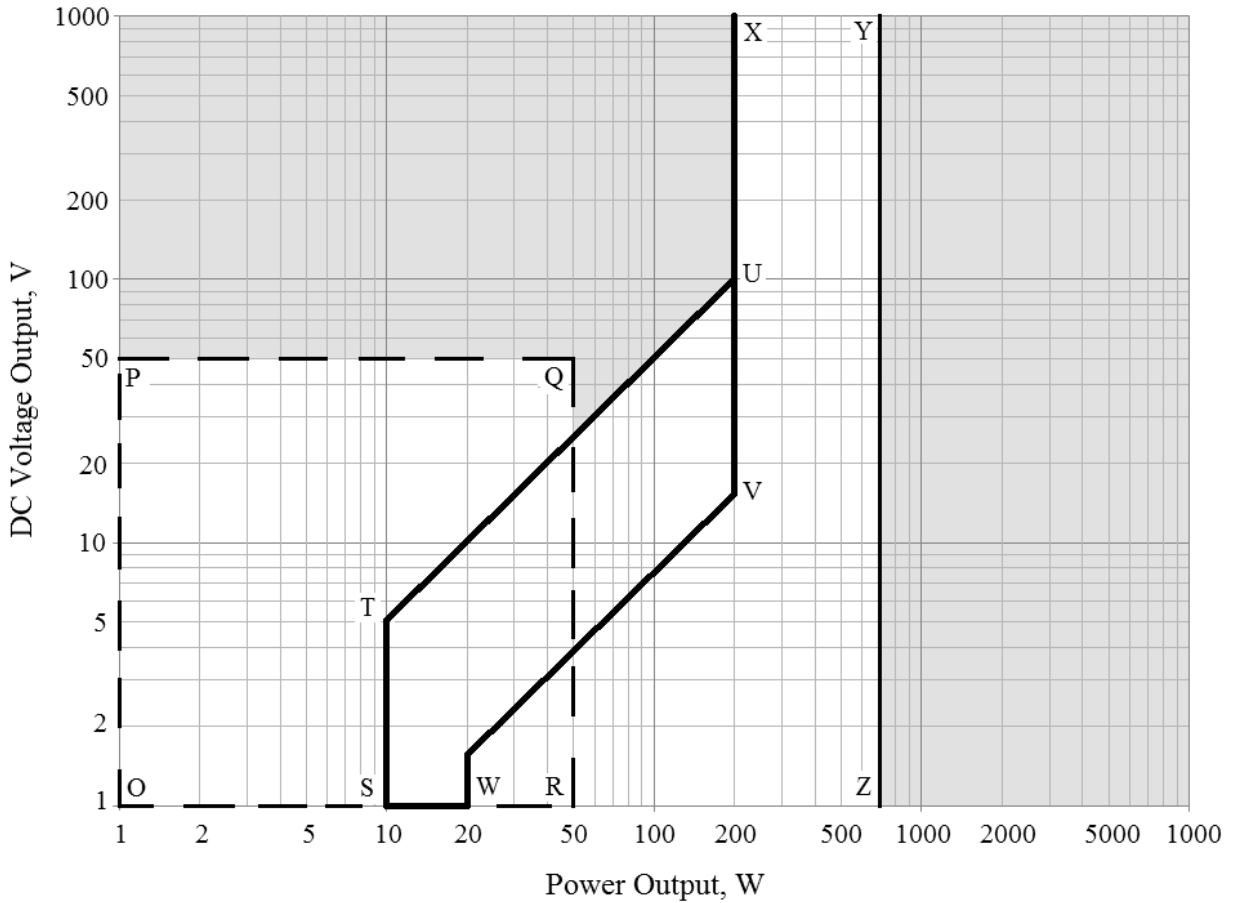


Fig. 7: Diagrammatic Comparison of Converters with Approximate Limits of Application

(Reproduced from [36])

Fly-back converters also happen to perform well within the rating represented by the shaded PQUXP. The transitional region rated within STUVWS is routine for different designs of fly-back and single-ended forward converters. The area enclosed between the boundaries of XUVWZYX mostly requires modified single-ended converter designs. For high output powers, in the shaded region to the right of the YZ vertical line, it is advantageous to use a push-pull forward converter circuit configuration. Because of the capability to meet high power requirements of implanted biomedical loads, single-ended and push-pull converters with frequency controlled configurations have been widely used for wireless energy transfer systems.

Active power converters are not considered the best choice for such applications as circuit components will require consumption of power from the wearable battery pack. In order to counterweigh the power loss, these converters are mostly designed with power amplifier configurations. Over the years, many standard converter amplifiers; for example, class E converters [8],[13],[15],[18],[19],[37] class D converters [39]-[44] have been proposed for transcutaneous power systems. The performance of these converter amplifiers has their own advantages and drawbacks that are influenced by impedance tuning of inductive or resonating coils, which is essential for maximum power transfer.

3.3.2 Tuning Topologies [45]

Use of inductive links for wireless data and power transmission applications such as powering implantable biomedical devices like cochlear implants, retinal implants, TAH, VAD etc. body area networks (BAN), wireless chargers and other telemetric applications demand efficient coupling links in order to maximize power transfer at low coupling ranges. Design requirements of an inductive link require careful consideration of voltage gain and power link efficiency. Power transfer is more efficient with high-frequency coils. The first step in the design and analysis of an inductive link requires simplified circuit representation of the inductive link. Inductive links may be driven either by a current or a voltage source. A most simple circuit can be represented using primary and secondary coil inductances and their self-resistances with a load impedance placed on the secondary circuit as shown in Fig. 8. This can be used to formulate a computational model for simulating the relationship of voltage gain and link efficiency to the coupling efficiency. The coupling efficiency is represented by coupling factor, k . Further decomposition of the primary and secondary impedance using resonating capacitors in both series and parallel configuration has significant effect on the link efficiency and voltage gain.

Also, complex controller circuit designs can be implemented to incorporate feedback in the link in order to perform a comprehensive frequency analysis on the resulting circuit.

Both inductive and resonance circuit topologies of transcutaneous power systems can be generalized with a voltage driven transformer circuit model with resonance impedances as shown in Fig 8. The depicted generalized model consists of respective L_1 and L_2 inductive coils at primary and secondary with their effective series resistances R_{L1} and R_{L2} . Also, Z_{1s} and Z_{2s} are usually capacitors that add series resonance impedances at primary and secondary side respectively. Z_{2p} is the parallel resonance impedance at the secondary side. Researchers usually choose to simplify Fig. 8 model with either tuning one of each or none of series and parallel impedances to achieve maximum link efficiency to transfer power wirelessly. These topologies can be categorized accordingly [45].

- i. No Resonance Topology
- ii. Series Tuned Primary Topology
- iii. Series Tuned Secondary Topology
- iv. Series Tuned Primary and Secondary Topology
- v. Parallel Tuned Secondary Topology
- vi. Series Tuned Primary and Parallel Tuned Secondary Topology

These topologies represent all possible circuit realizations to stabilize voltage driven inductive link. However, every topology has its own pros and cons in terms of voltage gain, efficiency, and other factors that affect power transfer efficiency. Parallel tuned secondary topology (Fig. 13) with a parallel resonating capacitor at the secondary side produces better efficiency as well as voltage gain for practical medical implant applications [46],[47]. Moreover, series tuned primary with parallel tuned secondary (Fig. 14) is a popular applied topology with

power amplifiers due to high voltage gain and efficiency characteristics at low coupling ranges. Voltage gain and link efficiency of series tuned primary with parallel tuned secondary (Fig. 14) is derived using Equation. (1) and Equation. (2) respectively [45].

The voltage gain in Equation (1) and efficiency in Equation (2) of this model (Fig. 14) is strictly dependent on the coupling coefficient, k as well as the system quality factor. In order to achieve maximum efficiency, the effective resistance of the coupled coils is usually designed to be as low as possible. This is achieved by optimized structural design of the interactive resonating coils.

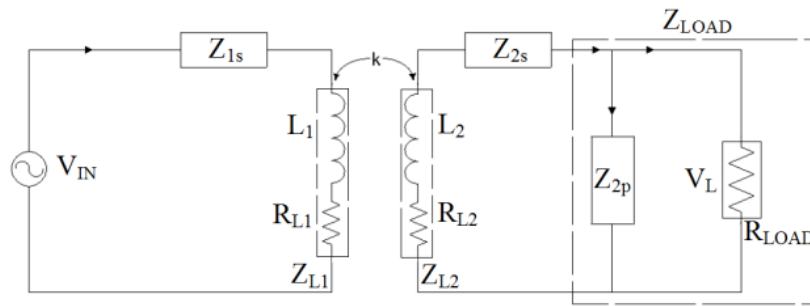


Fig. 8: Voltage Driven Generalized Model of Inductive Link

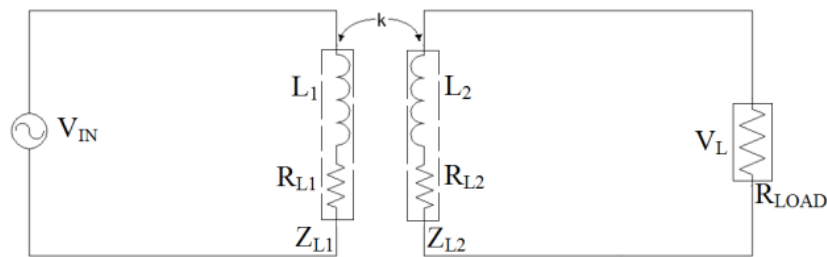


Fig. 9: No Resonance Topology

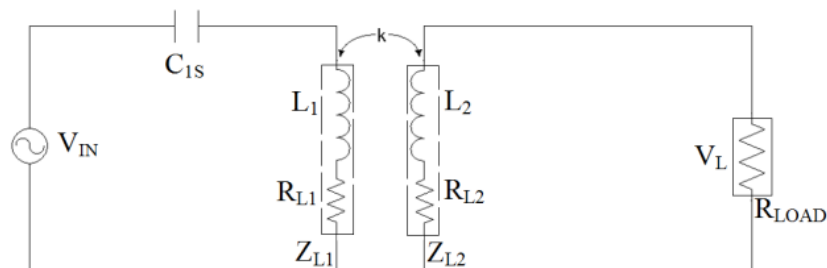


Fig. 10: Series Tuned Primary Topology

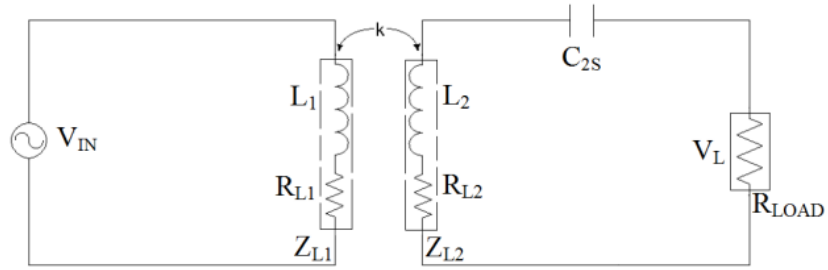


Fig. 11: Series Tuned Secondary Topology

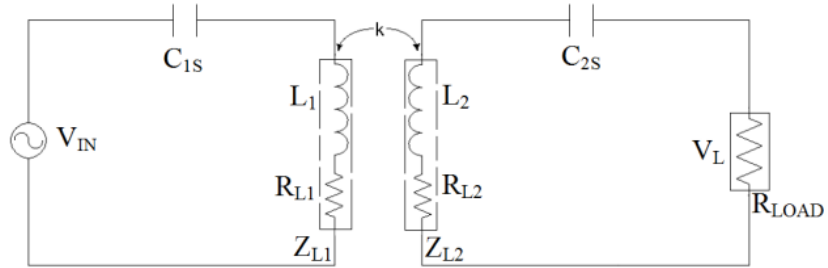


Fig. 12: Series Tuned Primary and Secondary Topology

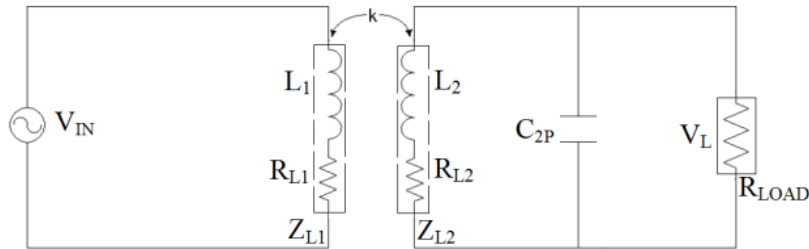


Fig. 13: Parallel Tuned Secondary

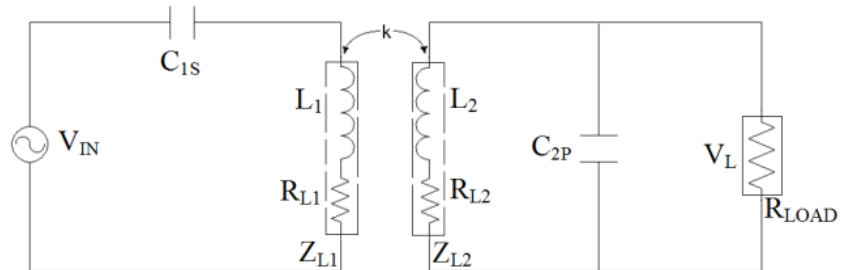


Fig. 14: Series Tuned Primary and Parallel Tuned Secondary Topology

$$\text{Gain} = \frac{V_L}{V_{IN}} = \frac{k\sqrt{L_1 L_2} C_{1s} R_{LOAD} \omega^2}{(C_{1s} R_{LOAD} C_{2p}(A)) \omega^4 + j(M)\omega^3 + (N)\omega^2 + j(O)\omega + (E)} \quad (1)$$

$$\text{Link Efficiency} = \eta_{\text{link}} = \frac{k^2 L_1 L_2 R_{LOAD} \omega^2}{R_{LOAD}^2 [(C_{2p}^2(K)\omega^4) + (R_{L1}(L) + F)\omega^2] + (R_{L1}(E)^2)} \quad (2)$$

Where,

k = coupling coefficient

$$A = k^2 L_1 L_2 - L_1 L_2$$

$$B = C + L_1 R_{LOAD} = (L_1 R_{L2} + L_1 R_{LOAD} + L_2 R_{L1})$$

$$C = L_1 R_{L2} + L_2 R_{L1}$$

$$D = R_{L1} R_{LOAD} + R_{L1} R_{L2}$$

$$E = R_{LOAD} + R_{L2}$$

$$F = (L_2^2 R_{L1} + k^2 L_1 L_2 (E))$$

$$G = (C_{2s}^2 R_{L1} (E)^2 - 2 R_{L1} L_2 C_{2s})$$

$$H = L_1 C_{1s} + L_2 C_{2s}$$

$$I = C_{2s} (E) + R_{L1} C_{1s} = C_{2s} (R_{L2} + R_{LOAD}) + R_{L1} C_{1s}$$

$$J = (L_1 + R_{L1} R_{L2} C_{2p})$$

$$K = (R_{L2} k^2 L_1 L_2 + L_2^2 R_{L1})$$

$$L = (C_{2p}^2 R_{L2}^2 - 2 C_{2p} L_2)$$

$$M = C_{1s} R_{LOAD} C_{2p} (C) - C_{1s} (A)$$

$$N = C_{1s} (B) + R_{LOAD} C_{2p} (R_{L1} C_{1s} R_{L2} + L_2)$$

$$O = R_{L1} C_{1s} (E) + R_{L2} C_{2p} R_{LOAD} + L_2$$

This generalized inductive link model to characterize all possible circuit realizations of a voltage driven inductive link depicts the relationship between the link efficiency and coupling coefficient. Resonating the secondary circuit by either series or parallel resonance remarkably improves the link efficiency and voltage gain. Also, resonance at primary side alters voltage gain only whereas resonance at secondary side alters both voltage gain and efficiency. Moreover, series resonating capacitor at the primary alters the voltage gain profile only. Other possibilities of tuning the primary side may include adding resonating parallel capacitors. The parallel capacitor will have the similar effect on changing the voltage gain as the series tuned capacitor in the primary. Overall, the series resonating impedance at the primary side causes voltage across the primary coil to increase and therefore, voltage developed at secondary side is increased proportionally. However, the ratio of voltage increase remains constant making the link efficiency stay constant. The use of tuning capacitor impedance in the design result in dependence on the operating frequency forcing the final circuit to be limited within a certain bandwidth.

Furthermore, transcutaneous power systems rely on the performance of the resonant circuits to transfer power under variable coupling and load conditions. Both voltage gain and link efficiency are dependent upon the coupling as well as the quality factor, Q that represents the load conditions.

$$Q = \frac{R_{load}}{\omega L_s}$$

Where R is the load resistance and ω is the operating angular frequency. A larger Q enables the system to be more tolerant to frequency mismatch of primary and secondary circuit [16],[47].

3.4 Summary

The design of a TET system using maximum power transfer requires tuning of impedance on both primary and secondary circuit. The DC converter is designed to excite the primary coil at a specific frequency; however, the pick-up frequency at the secondary is mostly lower but close to the primary. Therefore, changing the impedance at the secondary ensures better link efficiency as well as voltage gain. Yet, this does not guarantee that maximum power is transferred to the load device. The ultimate goal is to transfer energy efficiently to the implanted battery at a steady rate. In order to achieve this, maximum power transfer conditions need to be implemented to the secondary circuit including the rectifier and regulator for power delivery to the load impedance. The rate of energy transfer to the load is adversely affected by coupling discrepancies due to the misalignments of the coils. Examination of the misalignments is fundamental to designing a TET system with high coupling as it commands comprehension for designing coil size as well as orientation and location of coil placement.

CHAPTER 4

OPTIMIZED GEOMETRY OF TRANSCUTAENOUS COILS

4.1 Introduction

Current research in development for improved transcutaneous power system design is mostly a tradeoff between the size of the coils, level of coupling, tolerance to changes in coil alignment and relative power transfer efficiency [10],[48]. For theoretical analysis, the concept of coupling factor is generally adopted as a design parameter because it does not depend on the number of coil turns. However, the coupling factor is relative to the change of mutual inductance of the coils due to misalignments as well as coil-shapes. Additionally, the changes in mutual inductance affecting the coupling can be attributed to surgical placement, posture, patient alignment and differences in body shape. [10] Hence, a theoretical analysis of the parameters that affect the mutual inductance is fundamental to the system design.

4.2 Electromagnetic Induction

Faraday's law of electromagnetic induction forms the fundamental principle of transcutaneous power systems. According to this law, electromagnetic induction occurs due to an electromotive force (EMF, ε) created by electric current across a conductor moving through a magnetic field (\vec{B}). This EMF, produced around a closed path, is proportional to rate of change of magnetic flux, Φ through any surface bound by that path. Similarly, as shown in Fig. 15; because of current flow in the primary coil L_p , an EMF ε_{sp} is generated due to flux Φ_{sp} passing through the secondary coil, L_s . With N_s turns in the secondary, analytically,

$$EMF, \varepsilon_{sp} \propto -N_s \frac{d\Phi_{sp}}{dt} \propto \frac{dI_p}{dt} \quad (3)$$

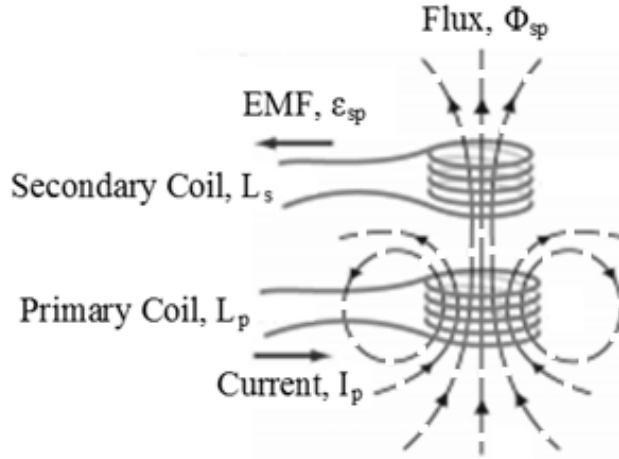


Fig. 15: Electromagnetic Induction

(Modified Image Extracted from MIT Physics 8.02 [49])

The minus sign is a consequence of Lenz's law stating that an induced current is always follows such a direction that its own magnetic field acts to oppose the effect that created it. The flux Φ_{sp} passing through the surface area of L_s is the number of the magnetic field lines passing through the surface area. Thus, coils with larger surface area will generate larger EMF as more flux can pass through them. Therefore, flux through small area dS_s is given by:

$$d\Phi_{sp} = \vec{B} \cdot d\vec{S}_s = B dS_s \cos\theta \quad \theta \neq 90^\circ \quad (4)$$

Using Stoke's theorem, the flux Φ_{sp} passing through secondary coil can be quantified using the magnetic vector potential, \vec{A}_s within its closed perimeter, \vec{l}_s :

$$\Phi = \iint_{S_s} \vec{B} \cdot d\vec{S}_s = \oint_{l_s} \vec{A} \cdot d\vec{l}_s \quad (5)$$

4.3 Coupling and Mutual Inductance

By definition, the mutual inductance, M between the secondary and primary coils is given by:

$$M = \frac{\Phi}{I_p} \quad (6)$$

Traditionally, the coupling factor k is expressed using the same mutual inductance as shown in Equation (7).

$$k = \frac{M}{\sqrt{L_p L_s}} \quad (7)$$

Where L_p and L_s respectively represent the self-inductance of the primary and secondary coil. L_p and L_s account for different coil shapes and sizes. The mutual inductance M changes according to oriental misalignments of the coils.

The proportionality constant, M in the relationship in Equation (3) is called the Mutual Inductance. Therefore by definition, mutual inductance of 1 Henry gives rise to an induced electromotive force of 1 Volt when current is changing at rate of 1 Ampere per second. For many simple circuits of only a few turns of wire, more convenient units are millinery (mH) and micrometry (uH). uH is much more appropriate for our study of small coils of few turns N_p and N_s . The adjective “mutual” emphasizes the fact that the E_{sp} , EMF produces I_s current flow in Coil L_s , magnetic flux created by Coil L_s is going to produce a same E_{ps} EMF in Coil L_p . Since this EMF is given rise by magnetic flux created by current flow in coils, a further study of definition of magnetic flux shows that mutual inductance depends on the alignment of the coils that is represented by $\cos\theta$.

$$\text{EMF in Coil } L_s, E_{sp} = -N_s \frac{d\Phi_{sp}}{dt}$$

$$N_s \frac{d\Phi_{sp}}{dt} \propto \frac{dI_p}{dt} \cong M_{21} \frac{dI_p}{dt}$$

$$E_{sp} = -N_s \frac{d\Phi_{sp}}{dt} = -M_{sp} \frac{dI_p}{dt}$$

$$M_{sp} = N_s \frac{\Phi_{sp}}{I_p}$$

$$\text{Flux in Coil, } \Phi_{sp} = \mathbf{B}_p \cdot \mathbf{Area}_s = \mathbf{B}_p \cdot \pi \mathbf{a}_s^2 = B_p \pi a_s^2 \cos\Theta$$

Due to Reciprocity,

$$\text{EMF in Coil } L_p, E_{ps} = -N_p \frac{d\Phi_{ps}}{dt}$$

$$N_p \frac{d\Phi_{ps}}{dt} \propto \frac{dI_s}{dt} \cong M_{ps} \frac{dI_s}{dt}$$

$$E_{ps} = -N_p \frac{d\Phi_{ps}}{dt} = -M_{ps} \frac{dI_s}{dt}$$

$$M_{ps} = N_p \frac{\Phi_{ps}}{I_s}$$

$$\text{Flux in Coil, } \Phi_{ps} = \mathbf{B}_s \cdot \mathbf{Area}_p = \mathbf{B}_s \cdot \pi \mathbf{a}_p^2 = B_s \pi a_p^2 \cos\Theta$$

Analytically, the coupling depends on the geometry of the coils that is the radii a_p and a_s as well as position of the coils with respect to each other. Therefore, insight research into the positioning of coils can predict efficiency of wireless power transfer using transformer coils. Using Equation (7), researchers usually preset a coupling factor within a range of 0.1 to 0.5 and measure the self-inductance L_p and L_s of coils. A coupling factor k is reported by all research as the resulting efficiency parameter. In this sense, the mutual inductance, M is deliberately not considered. This mutual inductance M can be defined using the size and geometric orientation of

alignment of the coils. The alignments can be generalized by separation distances and inclined angles while the coil are placed relative to each other.

4.4 Coil Alignment Scenarios

Several methods have been adopted by researchers and engineers over the years for identifying best methods to calculate mutual inductance with accuracy in various applications. For practical analysis, mutual inductance formulas using two single circular loops with different scenarios are idealized. In these studies, the primary coil is generalized to be still and a complete degree of freedom is applied to the secondary coil. Maxwell derived formulas for two circles with intersecting axes [50], Butterworth [51] and Snow [52] further developed formulas for circular loops with parallel axes. Based on these foundation studies, Grover developed a general method to calculate mutual inductance between inclined coils with arbitrary dimensional orientation [53],[54]. Babic et al. [55] a proposed new generalized mutual inductance formulas thoroughly validate all the noted studies using MIT developed FastHenry software [55].

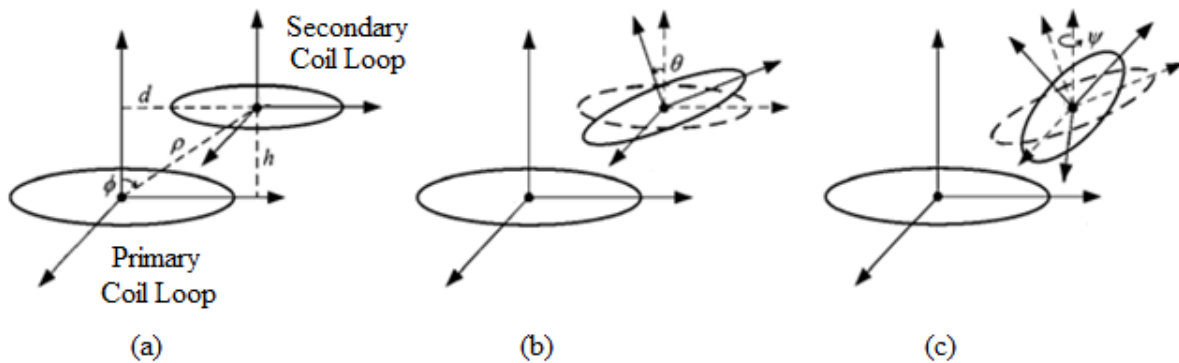


Fig. 16: Arbitrary Positioning of the Secondary Coil (a) Lateral Misalignment Only (b) Lateral and Inclined Angular Misalignment (c) Arbitrary Lateral and Inclined Angular Misalignment.

(Reproduced from IEEE Trans. Magn. [55])

Mutual inductance is proportional to the radii of the corresponding coils. However, considering the arbitrary positioning of the secondary coil as shown in Fig. 16; four parameters are good enough to describe the arbitrary position of the secondary coil representing how the coils are placed relative to their centers – (i) horizontal distance, h and (ii) vertical distance, d (iii) in-plane tilt angle, θ and (iv) rotation angle around axis, ψ .

All in all, for optimized mutual inductance calculation using Equation (8), Fig. 17 scenario can be considered by using two parameters $\frac{a_s}{a_p}$ and $\frac{h}{a_p}$ where primary and secondary coils with respective radii a_p and a_s are center aligned and parallel to each other and separated by a distance h . [54],[56]

$$M = f\sqrt{a_p a_s} \quad (8)$$

Here, f is a proportionality factor that is our point-of-interest for representing the misalignment characteristics. A relative comparison between Equation (7) and Equation (8) justifies that the size of the coils represented by radii a_p and a_s can be used for defining the self-inductance L_p and L_s .

Transcutaneous coils are mostly multi-layered and pancake-shaped. A general formula to calculate the self-inductance, L_M has been provided by Artan et. al. [9]

$$L_M = \sum_{i=1}^S \left(L_i + \sum_{1 \leq j \leq S; j \neq i} M_{ij} \right)$$

Where, S is the total number of layers, M_{ij} is the mutual inductance between two single layer coils. L_i is the self-inductance of the coil at layer i which can be calculated by the following equation.

$$L = \frac{\mu_0 N^2 r_{avg}}{2} \left(\ln \left(\frac{2.46}{\tau} \right) + 0.2\tau^2 \right)$$

Where, N is the number of turns in the coil, and τ and r_{avg} are calculated using the outer and inner radius of the coils accordingly.

$$\tau = \frac{r_{out} - r_{in}}{r_{out} + r_{in}} \quad r_{avg} = \frac{r_{out} + r_{in}}{2}$$

For ease of analysis, study of single layer coil self-inductance and mutual inductance is adopted to account for the misalignments. Fig. 17 – Fig. 21 shows all possible alignment scenarios of the two coils. Instead of using Equation (7), the size of the coils and these adaptive techniques of geometric orientation of the coils are used to derive mutual inductance M or M_{ij} for sufficient discretization. [54]

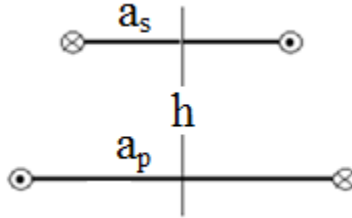


Fig. 17: Secondary coil is parallel and center aligned separated by vertical distance

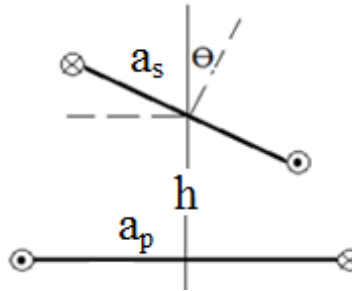


Fig. 18: Secondary coil center aligned with an inclined angle

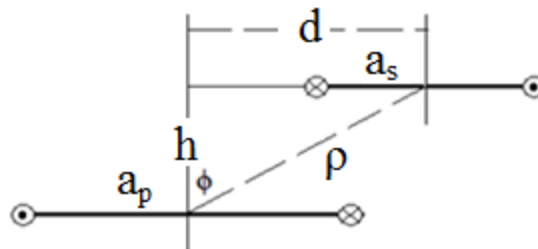


Fig. 19: Secondary coil is parallel and has a lateral alignment

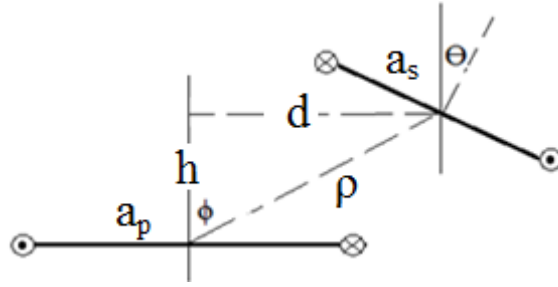


Fig. 20: Secondary coil has a lateral alignment with inclined angle

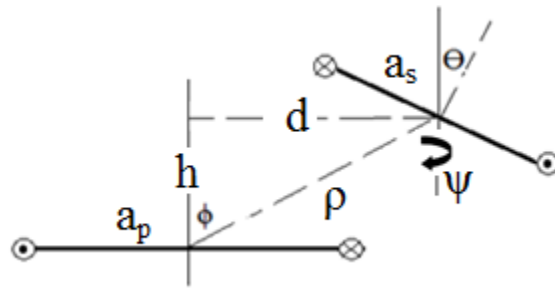


Fig. 21: Secondary coil is rotational in a lateral alignment with inclined angle

The term f in Equation (8) is obtained from a function of a variable k' . An appropriate depiction of k' is derived by finding the vector potential of the primary loop of coil with reference to the secondary loop [54],[56]. Theoretically, the coupling increases when the coils are placed close to each other as depicted in Fig. 17 where the coils are center aligned and parallel to each other. Using this scenario, Fig. 17 and Fig. 22, vector potential A due to current I_p in primary loop is derived by:

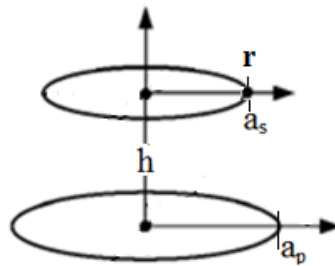


Fig. 22: Vector Potential of Primary Loop with reference to Secondary Loop

$$A = \frac{\mu_0 I_p}{\pi m} \sqrt{\frac{a_p}{a_s}} \left[\left(1 - \frac{m^2}{2}\right) K(m^2) - E(m^2) \right]$$

$$K(m^2) = \int_0^{\frac{\pi}{2}} (1 - m^2 \sin^2 \gamma)^{-\frac{1}{2}} d\gamma = \text{Complete Elliptical Integral of the First Kind}$$

$$E(m^2) = \int_0^{\frac{\pi}{2}} (1 - m^2 \sin^2 \gamma)^{\frac{1}{2}} d\gamma = \text{Complete Elliptical Integral of the Second Kind}$$

$$m^2 = \frac{4a_p a_s}{(a_p + a_s)^2 + h^2} = 1 - k'^2$$

$$k' = \sqrt{\frac{\left(1 - \frac{a_s}{a_p}\right)^2 + \left(\frac{h}{a_p}\right)^2}{\left(1 + \frac{a_s}{a_p}\right)^2 + \left(\frac{h}{a_p}\right)^2}} = \sqrt{\frac{(a_p - a_s)^2 + h^2}{(a_p + a_s)^2 + h^2}} \quad (9)$$

By Equation (8), a first-order approximation to optimize M is generally implemented by maximizing f. Relationship between f and k' has been intensely studied by physicists and RF (Radio Frequency) engineers. This relationship is represented by an approximate derivation of proportionality factor f using k' that depends on radii a_p, a_s and separating distance h (Equation (9)). Value of k'² ranges from 0 to 1.

It is traditional to adopt any of several methods available to calculate mutual inductance depending on certain ranges of k'². Table 2 shows a comparison of range of values k' within which several approximations of f is derived by researchers before [54].

Approximation by	Range of k'
Weinstein	0 to 0.25
Maxwell	0 to 0.75 and 0.98 to 1
Havelock	0 to 0.4 and 0.9 to 1
Nagaoka	0.04 to 0.4 and 0.3 to 1
Mathy	0.65 to 0.75

Table 2: Approximation of Proportionality Factor f within k' Range by Several Physicists

Two data sets in Appendix A and Appendix B have been commonly used for obtaining f from k'^2 by interpolation. Appendix A is provided by Grover et. al. [54] and Appendix B is adopted from RF Engineering Handbook by Henney et. al. [56]. A comparative graphical representation between the two is shown in Fig. 23.

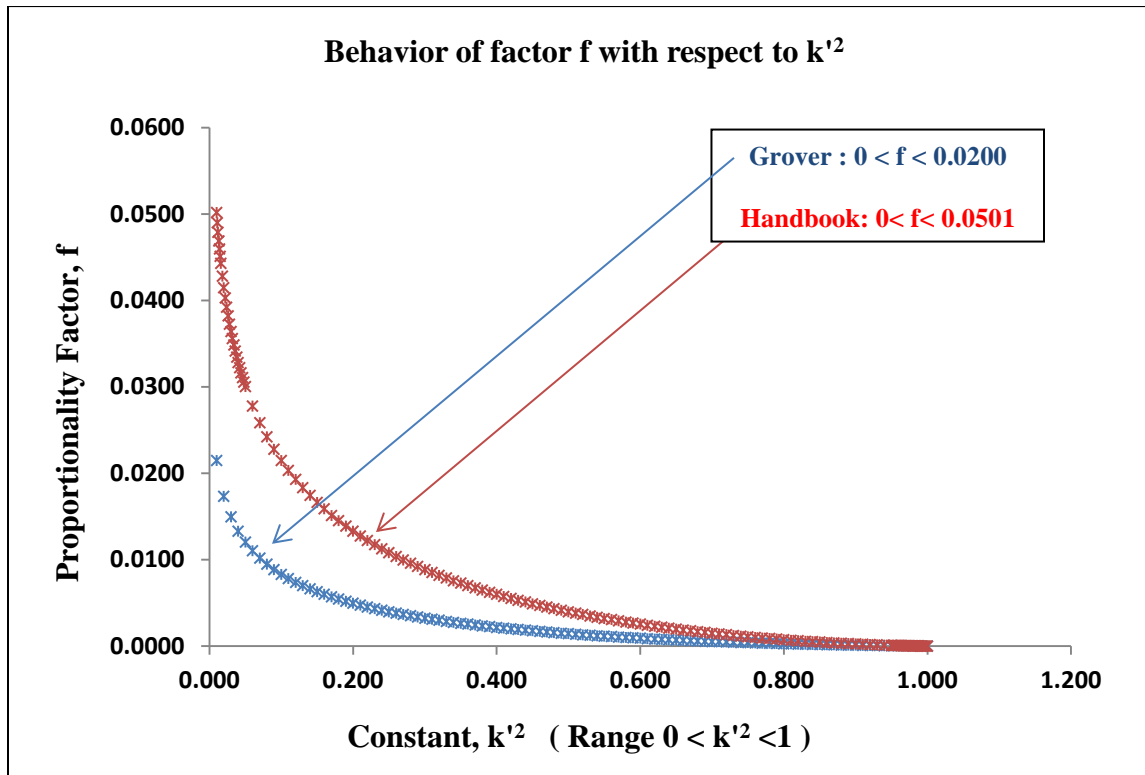


Fig. 23: Behavior of f with respect to k'^2 in Calculation of Mutual Inductance of Circular Coils

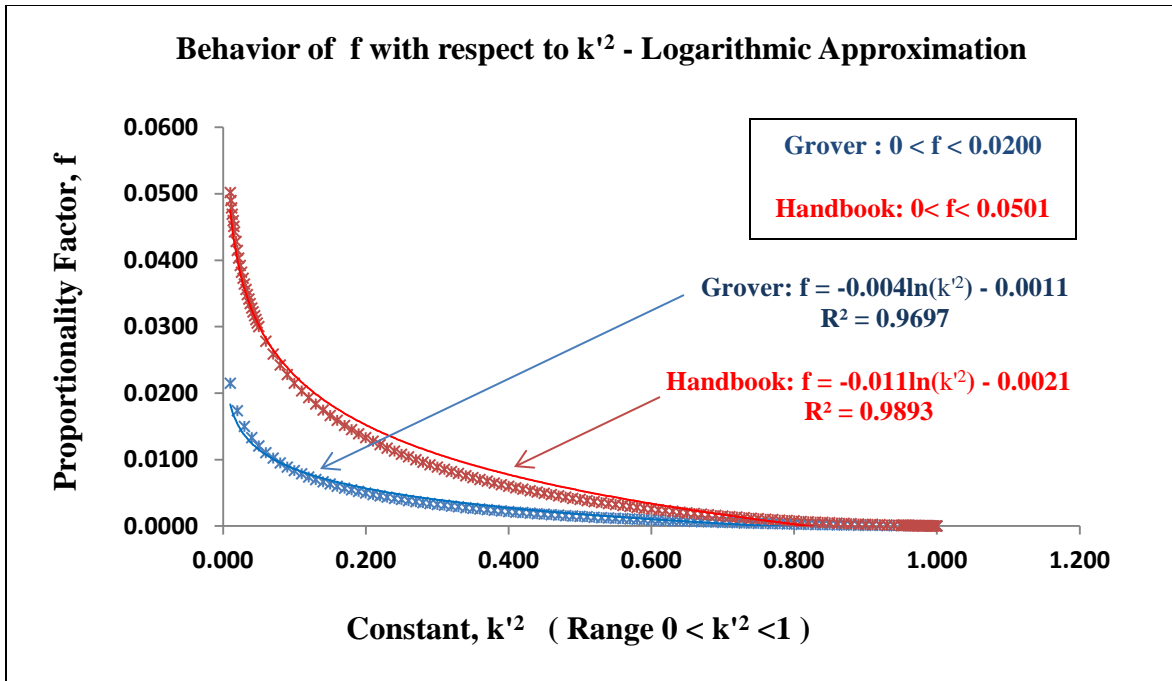


Fig. 24: Behavior of f with respect to k^2 - Logarithmic Approximation

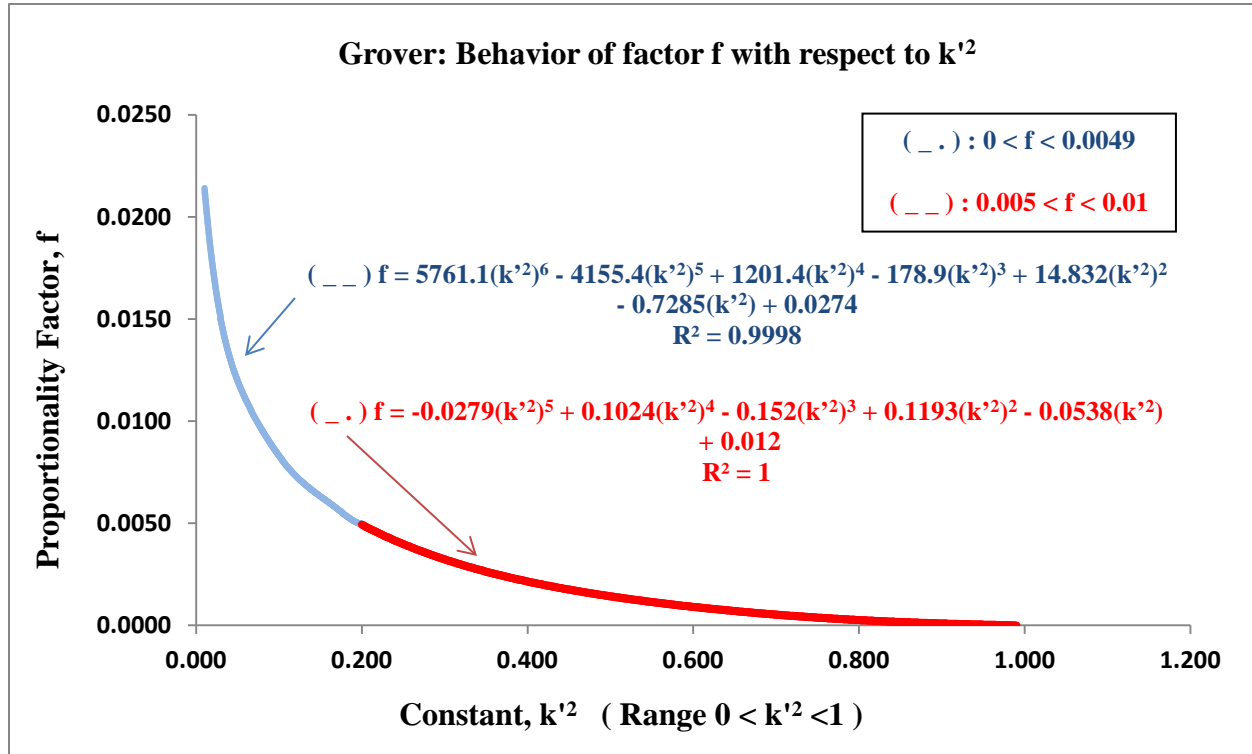


Fig. 25: Behavior of f with respect to k^2 - Distributed Approximation (Grover)

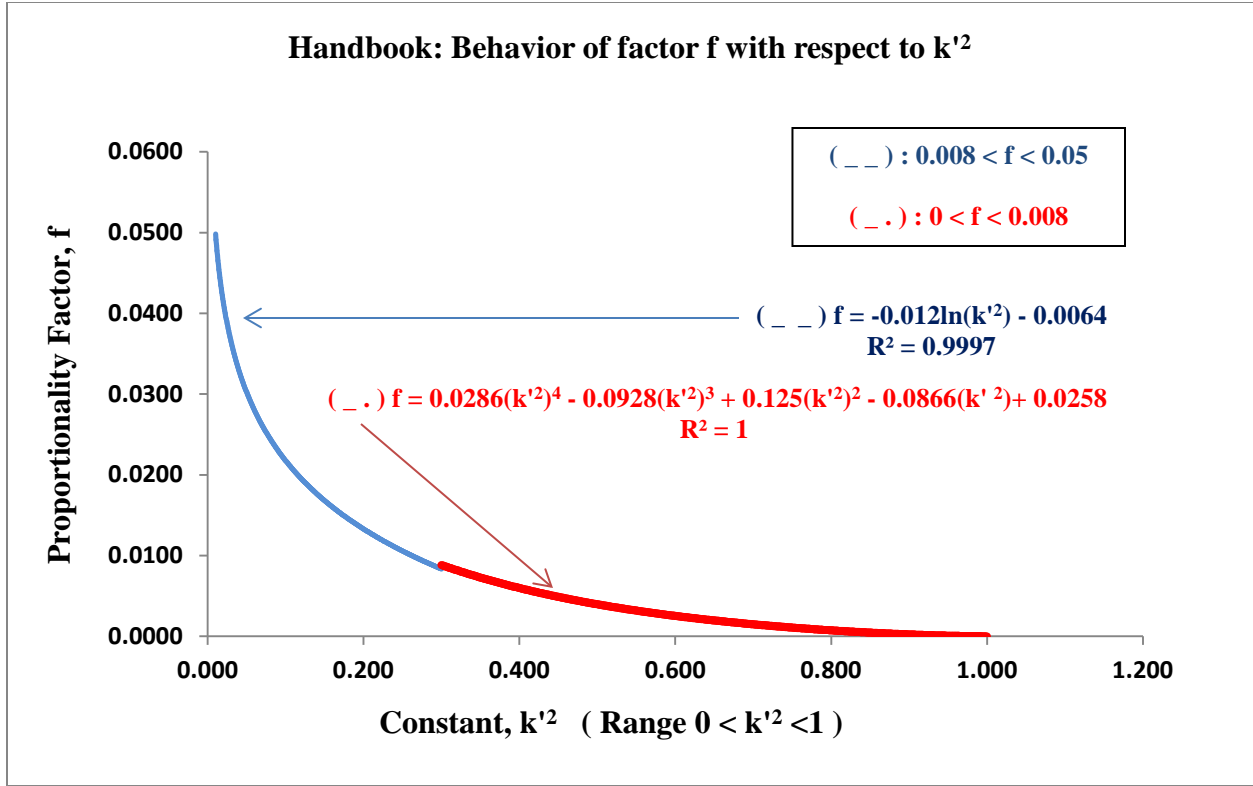


Fig. 26: Behavior of f with respect to k² - Distributed Approximation (RF Handbook)

Fig. 24, Fig 25, and Fig. 26 shows possible approximation of f relative to k' using regression. The regression equations are not discrete as the variable k' consists of arbitrary values of the radii and the separating distance. These approximate regressions are only fitting to calculate mutual inductance between coils separated by a distance of 10-15 centimeters. The logarithmic approximation in Fig. 24 can be considered best of the presented regression as it is a suitable estimation of Coffin's formula (Equation (10)) for calculating mutual inductance, M.

$$M = \sqrt{a_p a_s} 4\pi \left[\left(\frac{2}{m} - m \right) K(m) - \frac{2}{m} E(m) \right] \quad (10)$$

$$f \approx 4\pi \left[\left(\frac{2}{m} - m \right) K(m) - \frac{2}{m} E(m) \right]$$

$$K(m) = \int_0^{\frac{\pi}{2}} (1 - m \sin^2 \gamma)^{-\frac{1}{2}} d\gamma = \text{Complete Elliptical Integral of the First Kind}$$

$$E(m) = \int_0^{\frac{\pi}{2}} (1 - m \sin^2 \gamma)^{\frac{1}{2}} d\gamma = \text{Complete Elliptical Integral of the Second Kind}$$

$$m^2 = \frac{4a_p a_s}{(a_p + a_s)^2 + h^2} = 1 - k'^2$$

Furthermore, using Fig. 21, an overall scenario can be used to formulate mutual inductance for arbitrarily positioned coils by Neumann's definition [54].

$$M = \sqrt{a_1 a_2} \cdot \frac{1}{2\pi} \int_0^{2\pi} \frac{[\cos\theta - \frac{d}{a_2} (\cos\psi \cos\varphi - \sin\psi \sin\varphi \cos\theta)]}{R^{3/2}} \cdot f \, d\varphi$$

$\psi \neq 90^\circ$ and $\theta \neq 90^\circ$

$$R = \sqrt{\{(1 - \cos^2\varphi \sin^2\theta) + 2 \frac{d}{a_2} (\sin\psi \sin\varphi - \cos\psi \cos\varphi \cos\theta) + \frac{d^2}{a_2^2}\}}$$

$$\text{for } 0.010 \leq k'^2 \leq 0.300$$

$$k'^2 = \frac{(1 - \alpha R)^2 + \zeta^2}{(1 + \alpha R)^2 + \zeta^2} \quad \alpha = \frac{a_2}{a_1} \quad \delta = \frac{h}{a_1} \quad \zeta = \delta - \alpha \sin\theta \cos\varphi$$

Factor f is maximized when k' is minimized for all different coil sizes and alignment scenarios depicted in Fig. 17 - Fig. 21. Equation 11 is the result of the first order approximation of Equation (9), providing with an optimized relationship between the radii and separating distance.

$$h = \sqrt{(a_p^2 - a_s^2)} \quad (11)$$

Here, separating distance h can be predetermined by potential anatomic location for coil placement. Therefore, selection of a smaller radius of a_s secondary coil for implantation inside

the body can be used to design the primary coil size and shape. The design size of coils depends on patient size, location of implant as well as selection of implantable devices for example neuroprosthetic stimulators, cardiac assist devices etc.

4.5 Summary

Optimized coil design with respect to its geometry and diverse analysis can predict mutual inductance (Equation (8)) as well as link efficiency (Equation (1) and (7)). This efficiency is corresponding to coupling coefficient, k whose value ranges from 0 to 1 where 1 represents complete power transfer. A practical TETS is designed with $k = 0.4$ to 0.6 ; further increase of k result in unwanted temperature increase of coils. Link between the coils is efficient for smaller separation distances. On the contrary, increasing the corresponding radii further improves the sensitivity of mutual inductance at the expense of efficiency because the coupling factor k would decrease as well. Coil size and their geometric alignment are used in this research to refer commendable methods for calculating mutual inductance and coupling factor between transcutaneous coils. This successfully leads to to evaluate the design of different coil shapes and sizes as well as potential anatomic location of coil placement.

CONCLUSION

A smaller secondary coil resonating at high frequency ensures better and efficient power transfer for TETS. Continuous and power supply rate to the rechargeable battery is mostly achieved by controlling current supply duty cycle at desired voltage reference. This involves impedance tuning in order to maintain the operating frequency at both primary and secondary side. Tuning primary impedance using a series capacitor and secondary impedance using a parallel capacitor ensures maximum power transfer. The present design and implementation progress of research in this field of study involves acute decision-making using simulations for determination of diverse circuit parameters for controller functions. Before clinical trial, a well-defined and distinct system design and implementation of transcutaneous power system practices state-of-art technology development and testing process. Decades of academic and industrial researches have motivated improvement of wireless power systems for medical implants as they ensure reduced risk of infection and patient discomfort, enhance mobility, lower cost of care delivery, and above all, improve quality of daily life during medical treatment. Wireless power delivery to implantable devices is not only a theory or possibility, but also has now become a remarkable reality.

This research reviews various design criteria and constraints of a transcutaneous power delivery system for implanted systems. Unlike others, this research generalizes different scenarios of coil misalignments that can affect the coupling link. Depending on the findings of the research, optimized coil size for different alignment scenarios can be specified prior to system design. Furthermore, analysis of maximum power transfer topologies contributes to evaluating link efficiency with respect to coupling factor. Understanding these concepts of the

misalignment scenarios with optimized power transfer topologies offers opportunities to consider design of different coil shapes and sizes as well as potential anatomic location of coil placement. Efficient and optimum energy transfer using electromagnetic coupling and resonance depends on its coil size, geometry and placement orientation that directly impacts mutual inductance of the coils. This research finding brings life to commendable computational model for calculating mutual inductance as well as coupling factor between transcutaneous coils.

REFERENCES

- [1] V. Sharma, S. V. Deo, J. M. Stulak, L. A. Durham III, R.C. Daly, L. M. Baddour, K. Mehra, and L.D. Joyce, "Driveline infections in left ventricular assist devices: implications for destination therapy," *The Annals of Thoracic Surgery*, vol. 94, pp. 1381-1386, Nov. 2012.
- [2] A. C. Anyanwu, S. Pinney, K. Hammond, K. Ashley, and D. Adams, "Poor outcomes resulting from ventricular assist devices implanted in hospitals without dedicated ventricular assist device programs," *Mechanical Circulatory Support 2011*, vol. 2, Jun 2011.
- [3] A. A. Danilov, G. P. Itkin, and A. O. Ustinov, "Experimental setup for studying wireless energy transfer using magnetic coupling in auxiliary circulation systems," *Biomedical Engineering*. Vol. 45, No. 6, pp. 221-224, Mar. 2012.
- [4] H. Y. Leung, D. M. Budgett, and P. Hu, "Reactive component selection for TET powered medical devices," *Proc. 33rd Annu. Int. Conf. IEEE Eng. Med. Biol. Soc.*, pp. 2913-2916, 2011.
- [5] B. H. Waters, A. P. Sample, P. Bonde, and J. R. Smith, "Powering a ventricular assist device (VAD) with the free-range resonant electrical energy delivery (FREE-D) system," *Proc. IEEE*, Vol. 100, pp. 138-149, Jan. 2012.
- [6] E. A. Rose, et al., "Long-term use of a left ventricular assist device for end-stage heart failure," *The New England Journal of Medicine*, vol. 345, pp. 1435-1443, Nov. 2001.
- [7] M. S. Slaughter, and T. J. Myers, "Transcutaneous energy transmission for mechanical circulatory support systems: history, current status, and future prospects" *Journal of Cardiac Surgery*, vol. 25, pp. 484-489, 2010.
- [8] M. Chaoui, R. Perdriau, H. Ghariani, and M. Lahiani, "Design of a class-E transcutaneous energy transmitter for an implantable system," *Microelectronics International*, vol. 29, no. 1, pp.

22-34, 2012.

[9] N. S. Artan, X. Li, R. Patel, C. Ning, N. Ludvig, and H. J. Chao, "Multi-layer coils for efficient transcutaneous power transfer," *Proc. 33rd Annu. Int. Conf. IEEE Eng. Med. Biol. Soc.*, pp. 3031-3034, 2011.

[10] H. Y. Leung, D. M. Budgett, and A. P. Hu, "Minimizing power loss in air-cored coils for TET heart pump systems," *IEEE J. Emerg. Sel. Topics Power Electron.*, vol. 1, no. 3, pp. 412-419, Sept. 2011.

[11] J. Ma, Q. Yang, and H. Chen, "Transcutaneous energy and information transmission system with optimized transformer parameters for the artificial heart," *IEEE Trans. Appl. Supercond.*, vol. 20, no. 3, pp. 798-801, Jun. 2010.

[12] B. Liangyu, T. Houjun, J. Nan, and G. Xin, "Optimal design of the TET system for achieving maximum power transfer," *Proc. Int. Conf. Biomedical Engineering and Computer Science (ICBECS)*, Wuhan, China, pp. 1-4, 2010

[13] Q. Ma, M. R. Haider, S. Yuan and S. K. Islam, "Power-oscillator based high efficiency inductive power-link for transcutaneous power transmission," *Proc 53rd IEEE Int. Midwest Symp. Circuits and Systems (MSCAS)*, pp. 537-540, 2010.

[14] K. Zou, X. Li, and H. Zhang, "Transcutaneous power link design for implanted systems," *Proc. 4th IEEE Int. Conf. on Nano/Micro Engineered and Molecular Systems*, pp. 763-766, Jan. 2009.

[15] Z. Haitao, L. Xiaoying, L. Guiyang, and W. Zhigong, "Design and experiments of transmitter for transcutaneous energy transmission," *Proc. 6th Int. Workshop on Wearable and Implantable Body Sensor Networks (BSN)*, pp. 292-295, 2009.

[16] T. Dissanayake, D. Budgett, A. P. Hu, S. Malpas, and L. Bennet, "Transcutaneous energy

transfer system for powering implantable biomedical devices,” *Proc. 13th Int. Conf. Biomedical Engineering (ICBME)*, vol. 23, pp. 235-239, 2009.

[17] Q. Chen, S. C. Wong, C. K. Tse, and X. Ruan, “Analysis, design and control of a transcutaneous power regulator for artificial heart,” *IEEE Trans. Biomed. Circuits Syst.*, vol 3, no.1, pp 23-31, Feb. 2009.

[18] W. H. Moore, D. P. Holschneider, T. K. Givrad, and J. I. Maarek, “Transcutaneous RF-powered implantable minipump driven by a class-E transmitter,” *IEEE Trans. Biomed. Eng.*, vol. 53, no. 8, pp. 1705-1708, Aug. 2006.

[19] G. Wang, Liu, M. Sivaprakasam, and G. A. Kendir. “Design and analysis of an adaptive transcutaneous power telemetry for biomedical implants. *IEEE Trans. Circuit Syst. I, Reg. Papers*, vol. 52, no. 10, pp. 2109-2117, Oct. 2005.

[20] P. Si, A. P. Hu, S. Malpas, and D. Budgett, “A frequency control method for regulating wireless power to implantable devices,” *IEEE Trans. Biomed. Circuits Syst.* vol. 2, no. 1, pp. 22-29, Mar. 2008.

[21] T. J. Myers, K. Robertson, T. Pool, N. Shah, I. Gregoric, and O. H. Frazier, “Continuous flow pumps and total artificial hearts: management issues,” *The Annals of Thoracic Surgery*, vol. 75, S79-S85, Jun. 2003.

[22] T.R. Gowrishankar, D. A. Stewart, G.T. Martin, and J. C. Weaver, “Transport lattice models of heat transport in skin without spatially heterogeneous, temperature-dependent perfusion,” *Biomedical Engineering Online*, vol. 3, no. 42, Nov. 2004.

[23] Z. Yuwei, H. Xueliang, T. Linlin, B. Yang, and Z. Jianhua, “Current research situation and developing tendency about wireless power transmission,” *Proc. 2010 Int. Conf. Electricla and Control Engineering (ICECE)*, pp. 3507-3511, 2010.

- [24] W. H. Hayt Jr. and J.A. Buck. *Engineering Electromagnetics*. The McGraw Hill Companies Inc., 2006.
- [25] J Wang, M. Gulari, and K.D. Wise, “An integrated position-sensing system for a MEMS-based cochlear implant,” *IEEE Int. Electron Devices Meeting. IEDM Technical Digest*, pp. 121-124, Dec. 2005.
- [26] N. Rodriguez, J. Weissberg, and J. Loeb, “Flexible communication and control protocol for injectable neuromuscular interfaces,” *IEEE Trans. Biomed. Circuits Syst.*, vol. 1, no. 1, pp 29-27, Mar. 2007.
- [27] B. Smith, Z. Tang, M. W. Johnson, S. Pourmehdy M. M. Gazdik, J. R. Buckett, and P. H. Peckham, “An Externally Powered, Multichannel Implantable Stimulator-Telemeter for Control of Paralyzed Muscle,” *IEEE Trans. Biomed. Eng.*, vol. 45, no. 4, pp. 463-475, Apr. 1998.
- [28] G. J. Suaning and N. H. Lovell, “CMOS neuro-stimulation ASIC with 100 channels, scalable output, and bidirectional radio-freq. telemetry,” *IEEE Trans. Biomed. Eng.*, vol. 48, pp. 248-260, Feb. 2001.
- [29] W. Liu, et al., “A neuro-stimulus chip with telemetry unit for retinal prosthetic device,” *IEEE J. Solid-State Circuits*, vol. 35, no. 10, pp. 1487-1497, Oct. 2000.
- [30] O. Atasoy, and C. Dehollain, “A study for remote powering of a knee prosthesis through inductive link,” *Proc. Conf. Ph.D. Research in Microelectronics and Electronics (PRIME)*, pp. 1-4, July 2010.
- [31] R. Jon, C. Eapen, A. Ashhok, N. Sahoo, and A. Kumar, “Wireless power transfer to the implantable drug delivery system using helical antenna with inductive coupling,” *Int. Journal of Engineering and Advanced Technology*, vol. 1, no. 5, pp. 242-245, Jun. 2012.
- [32] K. Fotopoulou, and B. W. Flynn, “Wireless powering of implanted sensors using RF

inductive coupling,” *Proc. 5th IEEE Conf. Sensors*, pp. 765-768, Oct. 2006.

[33] S. Haj-Yahia, et al., “Midterm experience with Jarvik 2000 axial flow left ventricular assist device,” *The Journal of Thoracic and Cardiovascular Surgery*, vol. 134, pp. 199-203, Jul. 2007.

[34] A El-Banayosi, L. Arusoglu, L. Kizner, M. Morshuis, G. Tenderich, W. E. Pae Jr., and R. Korfer, “Preliminary experience with the LionHeart left ventricular assist device in patients with end-stage heart failure,” *The Annals of Thoracic Surgery*, vol. 75, pp 1469-1475, May 2003.

[35] The IEEE Standard for Safety Levels with Respect to Human exposure to Radio-Frequency Electromagnetic Field, 3KHz to 300GHz. *IEEE Xplore Digital Library*. 1991.

[36] O. Kilgenstein. *Switched-mode power supplies in practice*. John Wiley and Sons Ltd. 1989.

[37] M. W. Baker, and R. S. Sarpeshkar, “Feedback analysis and design of RF power links for low-power bionic systems,” *IEEE Trans. Biomed. Circuits Syst.*, vol. 1, no. 1, pp 28-38, Mar. 2007.

[38] N. Chaimanonart, K. R. Olszens, M. D. Zimmerman, W. H. Ko, and D. J. Young, “Implantable RF power converter for small animal in vivo biological monitoring,” *Proc. 27th Annu. Conf. Eng. Med. Bio. Soc.*, pp. 5194-5197, Jan. 2005.

[39] P. Wambsganss, and D. Huwig, “Inductive power transmission system with stabilized output voltage,” *Proc. 14th Int. Power Electronics and Motion Control Conf. (EPE/PEMC)*, pp. s15-1-s15-8, 2010.

[40] W. Ying, Y. Luguang, and X. Shangang, “Modeling and performance analysis of a new contactless power supply system,” *Proc. 8th Int. Conf. Electrical Machines and Systems*, vol. 3, pp. 1983-1987, Sept. 2005.

[41] S. Shabou, N. Rekik, M. Ghorbel, A. B. Hamida and M. Samet, “Conception of an emitter for transcutaneous power and high-speed data transmission,” *Proc. 16th Int. Conf.*

Microelectronics, pp. 655-659, Dec. 2004.

[42] G. B. Joun, and B. H. Cho, "An energy transmission system for an artificial heart using leakage inductance compensation of transcutaneous transformer," *IEEE Trans. Power Electron.*, vol. 13, no.6, pp 1013-1022, Nov. 1998.

[43] C. G. Kim, and B. H. Cho, "Transcutaneous energy transmission with double tuned duty cycle control," *Proc. 31st Intersociety Energy Conversion Engineering Conf.* vol. 1, pp. 587-591. Aug. 1996.

[44] A. Ghahary, and B. H. Cho, "Design of a transcutaneous energy transmission system using a series resonant converter," *Proc. 21st Annu. Power Electronics Specialists Conf.* pp 1-8, Jun. 1990.

[45] H. Ali, T. J. Ahmad, and S. A. Khan, "Mathematical modeling of an inductive link for optimizing efficiency," *Proc. IEEE Symp. Industrial Electronics and Applications (ISIEA)*, Kuala Lumpur, Malaysia, vol. 2, pp. 831-835, 2009.

[46] G. B. Hmida, H. Ghairani and M. Samet, "Design of a Wireless Power and Data Transmission Circuits for Implantable Biomicrosystem," *Biotechnology*, vol. 6, pp. 153-164, 2007.

[47] T. D. Dissanayake, D. M. Budgett, , P. Hu, , L. Bennet, , S. Pyner, L. Booth, , S. Amirapu, , Y. Wu, and S. C. Malpas, "A novel low temperature transcutaneous energy transfer system suitable for high power implantable medical devices: performance and validation in sheep," *Artificial Organs*, vol. 34, pp. 160-167, May 2010.

[48] R. Puers, and G. Vandevoorde, "Recent progress on transcutaneous energy transfer for total artificial heart systems," *Artificial Organs*, vol. 25, pp. 400-405,. 2001.

[49] S. Liao, P. Dourmashkin, and J. W. Belcher. *MIT Physics 8.02 Electricity & Magnetism*

[Online]. Available: <http://web.mit.edu/8.02t/www/802TEAL3D/visualizations/coursenotes/>

[50] J. C. Maxwell, *A Treatise on electricity and magnetism*. New York: Dover, 1954, (reprint from the original 1873).

[51] S. Butterworth, "On the coefficient of mutual induction of eccentric coils," *Phil. Mag.*, ser. 6, vol. 31, pp. 443-454, 1916.

[52] C. Snow, *Formulas for computing capacitance and inductance*, National Bureau of Standards Circular 544. Washington DC, Dec. 1954.

[53] F. W. Grover, "The calculation of the mutual inductance of circular filaments in any desired positions," *Proc. IRE*, pp. 620-629, Oct. 1944.

[54] F. W. Grover. *Inductance Calculations*. Dover Ed. New York: D. Van Nostrand. 1946.

[55] S. Babic, F. Sirois, C. Akyel, and C. Girardi, "Mutual inductance calculation between circular filaments arbitrarily positioned in space: alternative to Grover's formula," *IEEE Trans. Magn.*, vol. 46, no. 9, pp. 3591-3600, Sept. 2010.

[56] K. Henney. *Radio Engineering Handbook*. NY: McGraw-Hill, 1950.

[57] Z. Hamici, R. Itti, and J. Champier, "A high-efficiency power and data transmission system for biomedical implanted electronic devices," *Measurement Science and Technology*, vol. 7, no. 2, pp. 192-201, Feb. 1996.

[58] H. H. Wu, A. P. Hu, S. C. Malpas, and D. M. Budgett, "Determining optimal tuning capacitor values of TET system for achieving maximum power transfer," *Electronics Letters*, vol. 45, no. 9, pp 448-449, Apr. 2009.

[59] K. A. Townsend, J. W. Haslett, T. K. K. Tsang, M. N. El-Gamal, and K. Iniewski, "Recent advances and future trends in low power wireless systems for medical applications," *Proc. 5th Int. Workshop System-on Chip for Real-Time Applications (IWSOC)*, pp. 476-481, 2005.

- [60] T. Deyle, and M. Reynolds, "PowerPACK: a wireless power distribution system for wearable devices," *Proc. 12th IEEE Int. Symp. Wearable Computers*, pp. 91-98, 2008.
- [61] R. Bhutkar, and S. Sapre, "Wireless energy transfer using magnetic resonance," *Proc. 2nd Int. Conf. on Computer and Electrical Engineering (ICCEE)*, vol. 1, pp. 512-515, 2009.
- [62] N. Yin, G. Xu, Q. Yang, J. Zhao, X. Yang, J. Jin, W. Fu, and M. Sun, "Analysis of wireless energy transmission for implantable device based on coupled magnetic resonance," *IEEE Trans. Magn.*, vol. 48, no. 2, pp 723-726, Feb. 2012.
- [63] P. Si, A. P. Hu, D. Budgett, S. Malpas, J. Yang, and J. Gao, "Stabilizing the operating frequency of a resonant converter for wireless power transfer to implantable biomedical sensors," *Proc. 1st Int. Conf. Sensing Technology*, pp. 477-482, Nov. 2005.
- [64] G. B. Arfken, and H. J. Weber. *Mathematical methods for physicists*. 6th Ed. San Diego, CA: Academic Press Elsevier Inc. 2005.
- [65] A. I. Pressman, K. Billings, and T. Morey. *Switching power supply design*. 3rd Ed. McGraw-Hill, 2009.
- [66] L. W. Miller, et al., "Use of a continuous-flow device in patients awaiting heart transplantation," *The New England Journal of Medicine*, vol 357, pp. 885-896, Aug. 2007.
- [67] Pagani F. D., et al., "Extended mechanical circulatory support with a continuous-flow rotary left ventricular assist device," *Journal of the American College of Cardiology*, vol. 42, pp. 312-321, Jul. 2009.
- [68] W. L. Holman, S. V. Pamboukian, D.C. McGiffin, , J. A. Tallaj, M. Cadeiras, and J. K. Kirklin, "Device related infections: Are we making progress?," *Journal of Cardiac Surgery*, vol. 25, pp. 478-483, Jul 2010.
- [69] A. L. Raymond, et al., "Obesity and left ventricular assist device driveline exit site

infection,” *American Society of Artificial Internal Organs*, vol. 56, pp. 57-60, 2010.

[70] J. G. Allen, E. S. Weiss, J. M. Schaffer, N.D. Patel, S.L. Ullrich, S.D. Russell, A. S. Shah and J. V. Conte, “Quality of life and functional status in patients surviving 12 months after left ventricular assist device implantation,” *The Journal of Heart and Lung Transplantation*, vol. 29, pp. 278-285, Mar. 2010.

[71], D. H. Monkowski, P. Axelrod, T. Fekete, T. Hollander, S. Furukawa and R. Samuel, “Infections associated with ventricular assist devices: epidemiology and effect on prognosis after transplantation,” *Transplant Infectious Disease: an Official Journal of the Transplantation Society*, vol. 9, pp 114-120, Jun. 2007.

[72] P. L. Kalantarov, *Inductance calculations*. Moscow, Russia: National Power Press, 1955.

[73] H. B. Dwight, *Electrical coils and conductors*. New York: McGraw-Hill, 1945.

[74] C. Falcon, “Low-power Transceivers Get Patients Mobile,” *Communications Engineer*, vol. 2, no. 3, pp. 40-43, 2004.

[75] S. Baker, S. King, and J. Welch, “Performance measures of ISM-band and conventional telemetry,” *IEEE Eng. Med. Bio. Mag.*, vol. 23, no. 3, pp. 27-36, May 2004.

[76] N. S. Artan, H. Vanjani, G. Vashist, Z. Fu, S. Bhakthavatsala, N. Ludvig, G. Medveczky, and H. J. Chao, “A high-performance transcutaneous battery charger for medical implants,” *Proc. Int. Conf. of the IEEE Eng. Med. Biol. Soc. (EMBC)*, Buenos Aires, Argentina, pp. 1581-1584, 2010.

[77] M. Watada, K. Iwawaki, T. Tamada, K. Ouchi, S. Takatani, and Y. Um, “The development of core-type transcutaneous energy transmission system for artificial heart,” *Proc. 27th Annu. Int. Conf. Eng. Med. Bio. Soc.*, vol.10, pp. 3849-3852. Sept. 2005.

[78] T. Takura, H. Ishiai, F. Sato, H. Matsuki, and T. Sato, “Basic evaluation of signal

transmission coil in transcutaneous magnetic telemetry system for artificial hearts,” *IEEE Trans. Magn.*, vol. 41, no. 10, pp. 4173-4175, Oct. 2005.

[79] H. G. Lim, Y. H. Yoon, C. W. Lee, I. Y. Park, B. S. Song and J. H. Cho, “Implementation of a transcutaneous charger for fully implantable middle ear hearing device,” *Proc. 27th Annu. Conf. IEEE Eng. Med. Bio. Soc.*, vol. 10, pp. 6813-6816, Sep. 2005.

[80] K. S. Guillory, A. K. Misener and A. Pungor, “Hybrid RF/IR transcutaneous telemetry for power and high-bandwidth data,” *Proc. 26th Annu. Int. Conf. IEEE Eng. Med. Bio. Soc.*, vol. 2, pp. 4338-4340, Sept. 2004.

[81] M. P. Theodoridis and S. V. Mollov, “Distant energy transfer for artificial human implants,” *IEEE Trans. Biomed. Eng.*, vol. 52, no. 11, pp. 1931-1938, Nov. 2005.

[82] N. M. Neihart, and R. R. Harrison, “Micropower circuits for bidirectional wireless telemetry in neural recording application,” *IEEE Trans. Biomed. Eng.*, vol. 52, no. 11, pp. 1950-1958, Nov. 2005.

[83] K. Iwawaki, M. Watada, S. Takatani and Y. Um, “The design of core-type transcutaneous energy transmission systems for artificial heart,” *Proc. 30th Annu. Conf. IEEE Industrial Electronics Society*, pp. 948-952, Nov. 2004.

[84] A. Homma, et al., “Current status of national cardiovascular center totally implantable artificial heart system,” *Proc. Annu. Conf. SICE*, pp. 436-441, August 2004.

[85] L. Zhao, C. F. Foo and K. J. Tseng, “A new structure transcutaneous transformer for artificial heart system,” *IEEE Trans. Magn.*, vol. 35, no. 5, pp. 3550-3552, Nov. 1999.

[86] T. H. Nishimura, T. Eguchi, A. Kubota, K. Hamamoto and M. Saito, “An improved transmission energy transformer for a non invasive rechargeable battery to artificial organs,” *Proc. 8th IEEE Int. Conf. on Electronics, Circuits and Systems (ICECS)*, pp. 1209-1214, 2001.

[87] K. Shiba, et al., "Efficiency improvement and in vivo estimation of externally-coupled transcutaneous energy transmission system for a totally implantable artificial heart," *Proc. IEEE Eng. Med. Bio. Soc.*, pp. 2503-2505, Oct. 1997.

[88] H. Matsuki, Y. Yamakata and N. Chubachi, "Transcutaneous DC-DC converter for totally implantable artificial heart using synchronous rectifier," *IEEE Trans. Magn.*, vol. 32, no. 5, pp. 5118-5120, Sept. 1996.

[89] H. Matsuki and M. Shiki, "Investigation of coil geometry for transcutaneous energy transmission for artificial heart," *IEEE Trans. Magn.*, vol. 28, no. 5, pp. 2406-2408, Sept. 1992.

APPENDIX A

k'^2	f	k'^2	f	k'^2	f	k'^2	f
0.010	0.02147400	0.260	0.00380500	0.510	0.00135850	0.760	0.00035450
0.020	0.01731500	0.270	0.00364900	0.520	0.00130040	0.770	0.00032950
0.030	0.01493700	0.280	0.00350000	0.530	0.00124430	0.780	0.00030540
0.040	0.01328400	0.290	0.00335900	0.540	0.00119000	0.790	0.00028230
0.050	0.01202600	0.300	0.00322400	0.550	0.00113740	0.800	0.00025998
0.060	0.01101700	0.310	0.00309500	0.560	0.00108650	0.810	0.00023859
0.070	0.01017900	0.320	0.00297100	0.570	0.00103730	0.820	0.00021806
0.080	0.00946400	0.330	0.00285300	0.580	0.00098970	0.830	0.00019840
0.090	0.00884300	0.340	0.00274000	0.590	0.00094360	0.840	0.00017959
0.100	0.00829700	0.350	0.00263170	0.600	0.00089900	0.850	0.00016162
0.110	0.00781000	0.360	0.00252760	0.610	0.00085580	0.860	0.00014450
0.120	0.00737100	0.370	0.00242760	0.620	0.00081410	0.870	0.00012821
0.130	0.00697400	0.380	0.00233150	0.630	0.00077360	0.880	0.00011276
0.140	0.00661100	0.390	0.00223910	0.640	0.00073450	0.890	0.00009815
0.150	0.00627800	0.400	0.00215020	0.650	0.00069660	0.900	0.00008438
0.160	0.00597000	0.410	0.00206460	0.660	0.00066000	0.910	0.00007146
0.170	0.00568500	0.420	0.00198210	0.670	0.00062460	0.920	0.00005940
0.180	0.00542000	0.430	0.00190260	0.680	0.00059030	0.930	0.00004824
0.190	0.00517300	0.440	0.00182590	0.690	0.00055710	0.940	0.00003798
0.200	0.00494100	0.450	0.00175190	0.700	0.00052510	0.950	0.00002866
0.210	0.00472300	0.460	0.00168050	0.710	0.00049410	0.960	0.00002035
0.220	0.00451800	0.470	0.00161160	0.720	0.00046420	0.970	0.00001312
0.230	0.00432500	0.480	0.00154510	0.730	0.00043530	0.980	0.00000708
0.240	0.00414200	0.490	0.00148080	0.740	0.00040740	0.990	0.00000249
0.250	0.00396900	0.500	0.00141860	0.750	0.00038050	1.000	0.00000000

Table 3: Grover's Approximation Data Set for k'

APPENDIX B

k^2	f	k^2	f	k^2	f	k^2	f
0.010	0.05016000	0.170	0.01510000	0.520	0.00364300	0.870	0.00036250
0.011	0.04897000	0.180	0.01449000	0.530	0.00348700	0.880	0.00031880
0.012	0.04787000	0.190	0.01387000	0.540	0.00333700	0.890	0.00027750
0.013	0.04687000	0.200	0.01328000	0.550	0.00319100	0.900	0.00023860
0.014	0.04594000	0.210	0.01273000	0.560	0.00305000	0.910	0.00020210
0.015	0.04507000	0.220	0.01221000	0.570	0.00291300	0.920	0.00016800
0.016	0.04426000	0.230	0.01171000	0.580	0.00278000	0.930	0.00013640
0.018	0.04278000	0.240	0.01124000	0.590	0.00265200	0.940	0.00010740
0.020	0.04146000	0.250	0.01079200	0.600	0.00252700	0.950	0.00008107
0.022	0.04027000	0.260	0.01036600	0.610	0.00240700	0.952	0.00007613
0.024	0.03918000	0.270	0.00995800	0.620	0.00229000	0.954	0.00007131
0.026	0.03818000	0.280	0.00957000	0.630	0.00217700	0.956	0.00006661
0.028	0.03725000	0.290	0.00919900	0.640	0.00206800	0.958	0.00006202
0.030	0.03639000	0.300	0.00884400	0.650	0.00196200	0.960	0.00005756
0.032	0.03558000	0.310	0.00850300	0.660	0.00185900	0.962	0.00005320
0.034	0.03482000	0.320	0.00817500	0.670	0.00176000	0.964	0.00004899
0.036	0.03411000	0.330	0.00786100	0.680	0.00166400	0.966	0.00004490
0.038	0.03343000	0.340	0.00755900	0.690	0.00157100	0.968	0.00004093
0.040	0.03279000	0.350	0.00726900	0.700	0.00148400	0.970	0.00003710
0.042	0.03218000	0.360	0.00698900	0.710	0.00139400	0.972	0.00003340
0.044	0.03160000	0.370	0.00672000	0.720	0.00131000	0.974	0.00002984
0.046	0.03105000	0.380	0.00646000	0.730	0.00122800	0.976	0.00002643
0.048	0.03052000	0.390	0.00621100	0.740	0.00115000	0.978	0.00002316
0.050	0.03001000	0.400	0.00597000	0.750	0.00107410	0.980	0.00002004
0.060	0.02775000	0.410	0.00573800	0.760	0.00100100	0.982	0.00001708
0.070	0.02584000	0.420	0.00551400	0.770	0.00093060	0.984	0.00001430
0.080	0.02420000	0.430	0.00529700	0.780	0.00086260	0.986	0.00001168
0.090	0.02276000	0.440	0.00508700	0.790	0.00079730	0.988	0.00000926
0.100	0.02148000	0.450	0.00488500	0.800	0.00073450	0.990	0.00000703
0.110	0.02032000	0.460	0.00469000	0.810	0.00067410	0.992	0.00000502
0.120	0.01928000	0.470	0.00450100	0.820	0.00061620	0.994	0.00000326
0.130	0.01832000	0.480	0.00431800	0.830	0.00056070	0.996	0.00000177
0.140	0.01743000	0.490	0.00414000	0.840	0.00050760	0.998	0.00000062
0.150	0.01661000	0.500	0.00396900	0.850	0.00045690	1.000	0.00000000
0.160	0.01586000	0.510	0.00380300	0.860	0.00040850		

Table 4: RF Handbook Approximation Data Set for k'

